J. Fluid Mech. (1976), *vol.* 75, *part* 1, *pp.* 81–112
Printed in Great Britain

An experimental study of the effects of Prandtl number on thermal convection in a rotating, differentially heated cylindrical annulus of fluid

By JAY S. FEIN† AND RICHARD L. PFEFFER

Geophysical Fluid Dynamics Institute and Department of Meteorology,
Florida State University, Tallahassee

(Received 17 November 1975)

This paper presents the results of experimental studies of the behaviour of different fluids (mercury, $Pr = 0{\cdot}0246$; water, $Pr = 7{\cdot}16$; and 5 cS silicone oil, $Pr = 63$) when each is contained in a rotating cylindrical annulus and subjected to an imposed radial temperature difference across the annulus. The results are summarized in the form of two-parameter regime diagrams (thermal Rossby number Ro_T *vs.* Taylor number Ta) at different Prandtl numbers Pr. The fluids are in contact above and below with rigid insulating boundaries. The range of thermal Rossby and Taylor numbers surveyed is $10^{-3} < Ro_T < 10$, $10^5 < Ta < 10^9$.

The regime diagram for water with a rigid upper lid in contact with the fluid resembles in certain respects the more familiar regime diagram for water with a free upper surface obtained by Fultz (1956) and by Fowlis & Hide (1965). Significant differences do, however, occur and are discussed in a separate paper by Fein (1973). The regime diagram for silicone oil possesses no lower symmetric regime within the range of thermal Rossby and Taylor numbers surveyed; that for mercury possesses no upper symmetric regime within the range surveyed. In mercury, turbulence is observed at high Rossby numbers. An experimental traverse across the regime diagram in which the imposed temperature difference is held constant at $\Delta T = 5\,^{\circ}\mathrm{C}$ and the rotation rate Ω is changed monotonically reveals a highly conductive temperature structure in mercury and a highly convective temperature structure in both water and silicone oil. The regular wave regime, which appears at all three Prandtl numbers, is found to shift towards higher Taylor and Rossby numbers with decreasing Prandtl number. As a result, a single point in two-dimensionless-parameter space ($Ro_T = 5 \times 10^{-1}$, $Ta = 1 \times 10^6$) lies in the upper symmetric regime for 5 cS silicone oil ($Pr = 63$), in the regular wave regime for water ($Pr = 7{\cdot}16$) and in the lower symmetric regime for mercury ($Pr = 0{\cdot}0246$).

1. Introduction

Much effort has been devoted during the last 25 years to studies of the behaviour of thermally driven fluids contained in rotating cylindrical annuli. For a fixed geometrical aspect ratio it is known that the characteristic behaviour

† Present address: Department of Meteorology, University of Oklahoma, Norman, Oklahoma 73069.

Symbol(s)	Units	Definition
(r, θ, z)	cm, rad, cm	Cylindrical polar co-ordinates of a point in the annular convection chamber
t	s	Time
$\mathbf{g} = (0, 0, -g)$	cm s^{-2}	Acceleration due to gravity (taken as 980 cm s^{-2})
$\mathbf{\Omega} = (0, 0, \Omega)$	rad s^{-1}	Uniform angular velocity of rotation of annulus
a, b	cm, cm	$a < r < b$ is horizontal extent of liquid in convection chamber
d	cm	Depth of fluid in convection chamber
$\overline{\rho}$	g cm^{-3}	$\overline{\rho} = \frac{1}{2}[\rho(r = a) + \rho(r = b)]$, where $\rho(r)$ is the density of the liquid
$\Delta\rho$	g cm^{-3}	$\Delta\rho = \rho(r = a) - \rho(r = b)$
$\overline{\kappa}$	cm^2 s^{-1}	$\overline{\kappa} = \frac{1}{2}[\kappa(r = a) + \kappa(r = b)]$, where $\kappa(r)$ is the thermometric diffusivity of the fluid
$\overline{\nu}$	cm^2 s^{-1}	$\overline{\nu} = \frac{1}{2}[\nu(r = a) + \nu(r = b)]$, where $\nu(r)$ is the kinematic viscosity of the fluid
$\overline{\alpha}$	°C^{-1}	$\overline{\alpha} = \frac{1}{2}[\alpha(r = a) + \alpha(r = b)]$, where $\alpha(r)$ is the coefficient of volume expansion of the fluid
ΔT	°C	$\Delta T = \overline{\alpha}^{-1}\Delta\rho/\overline{\rho}$ is the externally imposed radial temperature difference $T(r = b) - T(r = a)$
$\overline{T}$	°C	$\overline{T} = \frac{1}{2}[T(r = b) + T(r = a)]$
Ro_T	—	$Ro_T = gd\Delta\rho/\overline{\rho}/\Omega^2(b-a)^2$
Ta	—	$Ta = 4\Omega^2(b-a)^4/\overline{\nu}^2$
Pr	—	$Pr = \overline{\nu}/\overline{\kappa}$

TABLE 1. Specification of the system, the imposed variables and the non-dimensional parameters

of such a fluid subjected to a radial temperature difference across the annulus is controlled primarily by three dimensionless parameters and by the boundary conditions. The three parameters are the Rossby number Ro_T, the Taylor number Ta and the Prandtl number Pr, each of which is defined in table 1. A convenient way of displaying the behavioural characteristics of the fluid as a function of these parameters is to construct two-parameter regime diagrams (Ro_T *vs.* Ta) corresponding to different Prandtl numbers. Most laboratory surveys to date, beginning with the work of Fultz (1956), have been limited to the use of water ($Pr \doteq 7$) as the working fluid with a free upper surface exposed to air. A notable exception was the work of Fowlis & Hide (1965), in which the transitions between the axisymmetric 'Hadley regime' and the quasi-geostrophic 'Rossby wave regime' were mapped for different liquids ($7{\cdot}19 \leqslant Pr \leqslant 62{\cdot}7$) with free upper surfaces.

More recently Fein (1973) investigated the effects of the upper surface boundary condition on the transitions between the Hadley and Rossby regimes and on the general character of the flow in the Rossby wave regime in water with a rigid lid in contact with the working fluid. In the present study we present similar data corresponding to experiments with silicone oil ($Pr = 63$) and with liquid mercury ($Pr = 0{\cdot}0246$). The basic data are in the form of temperature measurements as a function of time at one or two points within the annular convection chamber. Small thermistors embedded within the convecting fluid were used for this purpose. The annulus geometry was fixed and all three fluids were in contact with a rigid lid at the upper surface. Using the data obtained from the

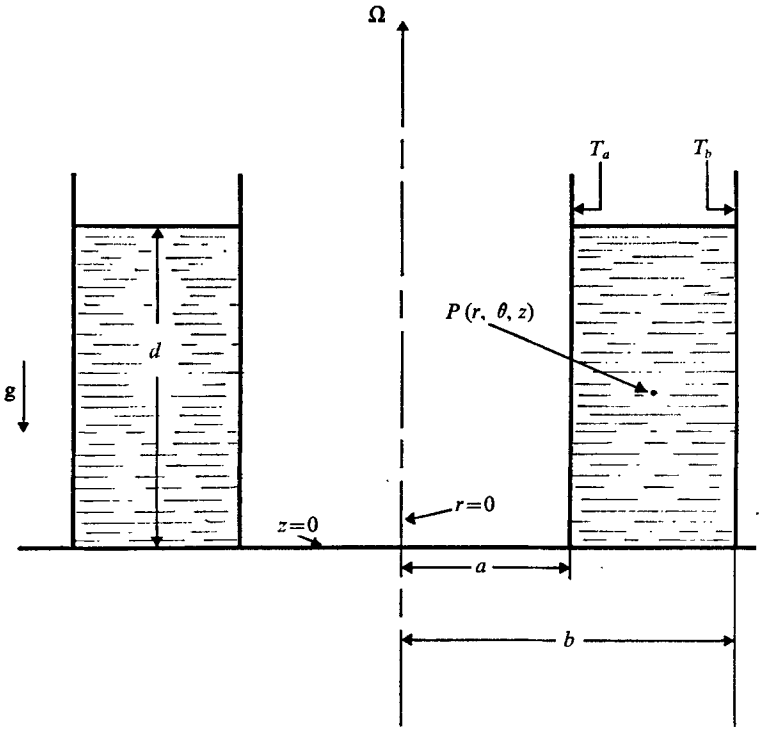

FIGURE 1. Schematic diagram of the differentially heated annulus of liquid. a denotes the radius of the inner cylinder, b the radius of the outer cylinder and d the depth of the liquid. T_a and T_b denote the temperatures of the inner and outer cylinders at a and b respectively. $P(r, \theta, z)$ denotes a point within the annulus rotating with an angular velocity $\boldsymbol{\Omega} = (0,0,\Omega)$ rad/s about the vertical axis. $\mathbf{g} = (0, 0, -g)$ cm/s^2 is the acceleration due to gravity.

thermistor measurements we have determined the amplitudes and phase speeds of the unstable waves and we have mapped the wavenumber transitions and the transitions between the symmetrical and wave regimes. We have also determined gross measures of the static stability and the Burger and Richardson numbers.

2. Apparatus and measurements

The annulus and auxiliary apparatus used in this study were identical to those used by Fein (1973). Since a rather complete description of the apparatus and measurements may be found in Fein's paper, we shall mention here only the major features of the experimental model which we feel are needed for a meaningful evaluation of the experimental results.

The annulus consisted of an annular ring of liquid confined between two concentric, vertical, thermally conducting, right circular cylinders which were maintained at uniform but different temperatures, with the outer cylinder always the warmer of the two (see figure 1). The base of the annular convection chamber was thermally insulating. The upper surface of the experimental liquid was in direct contact with a thermally insulating lid. The annulus rotated counterclockwise at a constant rate Ω about a vertical axis. The dimensions of the annulus

were as follows: inner radius $a = 3{\cdot}48$ cm, outer radius $b = 6{\cdot}02$ cm, depth $d = 5{\cdot}00$ cm.

All temperature measurements within the annular convection chamber were made at the mid-radius $r = \frac{1}{2}(b+a)$ by means of either one or two small thermistor probes. Most measurements were made at the mid-depth. The exceptions were a limited number of static-stability measurements. For the latter purpose two thermistors were aligned vertically at $d = 0{\cdot}40$ cm and $d = 4{\cdot}60$ cm. When measurements were made at the mid-depth, two different methods were used, depending upon whether the thermal waves were nearly stationary or drifting significantly with an angular velocity relative to the basic angular velocity of the annulus.

Drifting waves were sensed by two thermistors (bead diameters $\doteq 1$ mm) suspended at the mid-radius and mid-depth by their own insulated copper leads (diameters $\doteq 0{\cdot}1$ mm). The thermistors were separated azimuthally by $\frac{1}{6}\pi$ rad. The wavenumbers and the angular velocity of the regular wave patterns were determined from the relative wave phases sensed by the two probes.

The static-stability measurements were made by means of a modified stationary probe arrangement with 1 mm thermistor beads mounted at the ends of two hypodermic tubes (diameters $\doteq 1$ mm) which were fitted through and supported by the rigid upper lid.

For cases in which the wave patterns were essentially stationary, a modified upper rigid lid was used. The mid-section of that lid, which supported a hypodermic tube with a thermistor bead at its lower end, was rotated in the direction of and at 1 rev/h relative to the angular velocity of the annulus. In 1 h, therefore, a complete azimuthal traverse was made of the stationary wave pattern. The wavenumber was determined simply as the number of waves (to the next higher integer) along that traverse.

Low level electrical signals from the thermistors were transferred from the rotating annulus to a multi-channel dynograph pen recorder via a high quality multi-channel electrical slip-ring.

Table 2 lists the range and uncertainty of measurement of the parameters associated with and measured by the apparatus discussed in this section.

3. Experimental procedure

Transition points between the upper symmetrical regime and the regular wave regime were determined by fixing the imposed temperature gradient ΔT and varying the rotation rate Ω in small steps (usually 2 % or less in the vicinity of the transition). A steady state (characterized by variations in thermal wave amplitude no greater than 0·01 °C and changes in wave period no greater than 10 % over a 1 h period) was attained at each step, and the type of convection (i.e. axisymmetric, wavelike or turbulent) was recorded.

Transitions between the lower symmetrical regime and the wave regime were determined by fixing Ω and varying ΔT in small steps (usually 20 % or less in the vicinity of the transition). A steady state was attained and the type of flow was recorded at each step.

Parameter	Range	Uncertainty
a (cm)	3·48	±0·4%
b (cm)	6·02	±0·2%
$b-a$ (cm)	2·54	±0·6%
d (cm)	5·00	±0·2%
Ω (rad/s)	0 to 10·0	±0·5%
ΔT (°C)	0·10 to 30·00	+50% (ΔT = 0·10 °C) to ±1%($\Delta T \geqslant$ 5·00 °C)
T (°C)	20·00	±0·2%
$\Delta\rho$ (g/cm³)	Mercury: $0{\cdot}50\times10^{-3}$ to $73{\cdot}8\times10^{-3}$	Same as ΔT
	Water: $0{\cdot}010\times10^{-3}$ to $5{\cdot}93\times10^{-3}$	Same as ΔT
	Oil: $0{\cdot}097\times10^{-3}$ to $29{\cdot}1\times10^{-3}$	Same as ΔT
$\bar{\rho}$ (g/cm³)	Mercury: 13·5	Negligible
	Water: 0·998	Negligible
	Oil: 0·925	Negligible
$\bar{\alpha}$ (°C^{-1})	Mercury: $1{\cdot}82\times10^{-4}$	Negligible
	Water: $2{\cdot}06\times10^{-4}$	Negligible
	Oil: $10{\cdot}5\times10^{-4}$	Negligible
$\bar{\nu}$ (cm²/s)	Mercury: $1{\cdot}14\times10^{-3}$	Negligible
	Water: $10{\cdot}1\times10^{-3}$	Negligible
	Oil: 55×10^{-3}	±2%
$\bar{\kappa}$ (cm²/s)	Mercury: $46{\cdot}3\times10^{-3}$	Negligible
	Water: $1{\cdot}41\times10^{-3}$	Negligible
	Oil: $0{\cdot}88\times10^{-3}$	±2%

TABLE 2. Range and uncertainty of measurement of the parameters. The values for $\bar{\rho}$, $\bar{\nu}$, $\bar{\kappa}$ and $\bar{\alpha}$ are from Fowlis & Rossby (1964) for water and mercury and from Dow Corning's *Electronic Materials* (1968, Midland Michigan) for oil

Transition points between the symmetric and regular wave regimes were defined as those points in parameter space at which the thermal amplitude of the first sustained wavelike perturbation was equal to or exceeded 0·01 °C.

Transitions between the regular and irregular wave regimes, as well as all but one transition between the regular wave regime and the turbulent regime in mercury, were determined by fixing ΔT and varying Ω in steps of approximately 10%. Finer resolution was not attempted because these transitions, unlike those between the symmetric and regular wave regimes, are not sharp and are therefore represented better by a zone rather than a line in parameter space.

Reversing the direction of the traverses in parameter space produced no noticeable differences in the critical values of the parameters at transitions.

The uncertainty limit assigned to a particular transition point was determined by (i) the magnitude of the step we chose in varying the independent parameters Ω and ΔT across that transition point, and (ii) the uncertainty associated with measuring Ω and ΔT at any one point in dimensionless parameter space.

Speed measurements were made in liquid mercury at several values of the rotation rate, at ΔT = 5·00 °C, within the regular wave regime and within the non-geostrophic turbulent regime. These measurements were accomplished by heating the thermistor above the ambient temperature and measuring the amount of cooling produced by the speed of the fluid moving by it. The techniques involved were discussed in depth by Fowlis (1970).

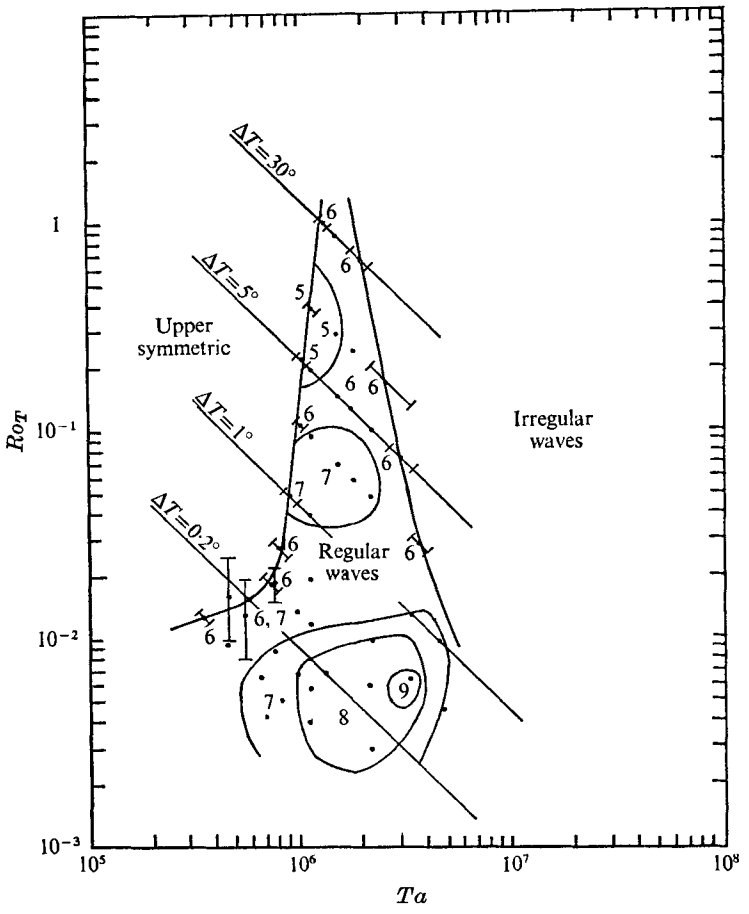

FIGURE 2. The regime diagram for silicone oil. The solid circles within the regular wave regime represent experimental points at which the thermal wavenumber, the amplitude and the angular drift rate were measured. The wavenumber regimes are depicted on the basis of a subjective analysis of the wavenumber data at these points. Experimental conditions: $b-a = 2{\cdot}54$ cm, $d = 5{\cdot}00$ cm, $\bar{T} = 20{\cdot}00$ °C, $\bar{\nu} = 5{\cdot}5 \times 10^{-2}$ cm²/s, $\bar{\kappa} = 8{\cdot}8 \times 10^{-4}$ cm²/s, $\bar{\alpha} = 1{\cdot}05 \times 10^{-3}$ °C^{-1}, $\bar{\rho} = 0{\cdot}925$ g/cm³, $Pr = 63$, upper surface rigid.

The reader is referred to Fein (1973) for a more thorough description of the experimental procedures used in this study.

4. Results for 5 cS silicone oil ($Pr = 63$)

The regime diagram

Figure 2 shows the regime diagram for silicone oil plotted in log–log co-ordinates in the parameter space (Ro_T, Ta). The ordinate Ro_T is proportional to $\Delta T/\Omega^2$ and the abscissa Ta is proportional to Ω^2. Therefore lines of constant ΔT are oriented at 45° to the axis, with Ω increasing downwards and towards the right along those lines. Lines of constant Ω are vertical and parallel to the Ro_T axis.

One striking feature of the regime diagram is that above $Ro_T = 3 \times 10^{-2}$ the

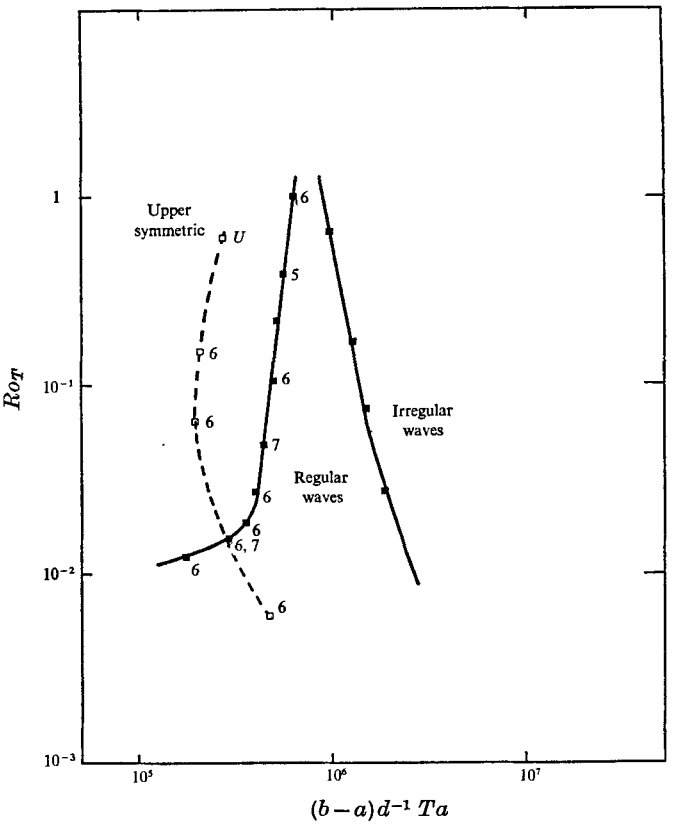

FIGURE 3. The regime diagrams for high Prandtl number fluids with and without a rigid upper surface. □, – – –, after Fowlis & Hide (1965), for a solution of glycerol and water (Pr = 62·7) with a free upper surface; ■, ——, from the present study, for silicone oil (Pr = 63) with a rigid upper surface.

	$b-a$	d	$\overline{\rho}$	$\overline{\alpha}$	$\overline{\nu}$	$\overline{\kappa}$
Fowlis & Hide	2·54	10·00	1·14	$4{\cdot}58\times10^{-4}$	$6{\cdot}80\times10^{-2}$	$0{\cdot}109\times10^{-2}$
Present study	2·54	5·00	0·925	$10{\cdot}5\times10^{-4}$	$5{\cdot}5\times10^{-2}$	$0{\cdot}088\times10^{-2}$

transition curve between regular waves and the upper symmetric regime is found to be only weakly dependent upon Ta. In comparison with the upper transition curve for water (see figure 21) this curve appears to have degenerated into an elongated 'knee' or viscous cut-off at $Ta \sim 10^6$. A similar result was reported by Fowlis & Hide (1965) for a glycerol–water solution (Pr = 62·7) with a free upper surface. Their transition data are plotted in figure 3 (dashed curve) along with those for the present study (solid curves). Because Fowlis & Hide's (1965) fluid depth was different from ours (10·00 cm *vs.* 5·00 cm), the curves in figure 3 are presented in the parameter space (Ro_T, $(b-a)\,d^{-1}Ta$) in order to scale out the depth dependence (see Fowlis & Hide 1965).

The presence of a rigid upper boundary apparently shifts the upper transition curve (for $Ro_T \geqslant 3\times10^{-2}$) towards higher values of Ta by a factor of approximately two, supporting the conclusion reached by Fein (1973) that the inclusion

of an additional 'rigid' Ekman layer (due to the introduction of the rigid upper boundary) should approximately double the Ekman-layer dissipation and thus displace the position of the 'knee' towards higher values of the Taylor number.

On the basis of the data of Fowlis & Hide (1965), shown in figure 3, one might have expected to find a lower symmetric regime at low values of Ro_T. We found instead that for a rigid lid in contact with the upper surface of the fluid the transition curve turns towards lower values of Ta as Ro_T is decreased. This result was first observed strictly by means of the rotating probe, since drift rates in this region of parameter space were very small. It was so unexpected, however, that the experiments were repeated using the stationary probe. The two sets of results were compatible. Although thermal wave amplitudes in these regions are very low and difficult to measure (generally only several hundredths of a degree centigrade) the experiments are quite convincing.

Figure 4 shows theoretical regime diagrams which are the unpublished work of Dr Paul Mason (1976), who has been kind enough to allow their publication here. Mason's theory is based on Hide's extension of Eady's theory to include Ekman boundary layers and sloping boundaries (Hide 1969). The theory which produced curve A takes into account Ekman-layer friction at rigid upper and lower boundaries (Barcilon 1964). The theory which produced curve B includes, in addition, the effect of the slope of the geopotentials (Hide & Mason 1975; Mason 1976). The imposed parameters correspond to the silicone-oil experiment (see figure 2). The large differences between curves A and B show that the slope of the geopotentials plays a vital role in this area of parameter space, and the agreement between curve B, compared with curve A, and figure 2 is quite pronounced.

Relative to the regime diagram for water the regular wave regime for silicone oil was 'compressed' in parameter space, especially at high values of Δt (see figure 21). The transition curve separating the regular and irregular wave regimes is essentially a straight line in log–log space for $\Delta T \geqslant 2{\cdot}40\,^{\circ}\mathrm{C}$. At and below $\Delta T = 1{\cdot}00\,^{\circ}\mathrm{C}$ regular waves were observed along an extension of this line, implying that the regular wave regime 'opens up' in those regions.

The wavenumber regimes

The regular wave regime for silicone oil as depicted in two-parameter space, Ro_T *vs.* Ta (figure 2), displays less regularity in structure than that for water (cf. Fein 1973). The range of wavenumbers observed in silicone oil, however, is smaller. Above $Ro_T \sim 10^{-2}$ a wavenumber of six predominates, probably owing to the geometry of the annulus. It should be noted in this connexion that the annular gap width $b-a$ was almost exactly equal to half the wavelength for a wavenumber of six, making this the most circular of all possible wavenumbers. To a lesser extent a wavenumber of six was also observed to predominate in water (see Fein 1973) and in mercury (see figure 9). We should also note that Fowlis & Hide (1965), whose gap width was identical to that for the present study, reported observing only a wavenumber of six for their $Pr = 62{\cdot}7$ experiment (see figure 3) in a fluid with a free upper surface.

The most salient feature of the regular wave regime shown in figure 2 is the wavenumber maximum located at low values of Ro_T, about mid-way across

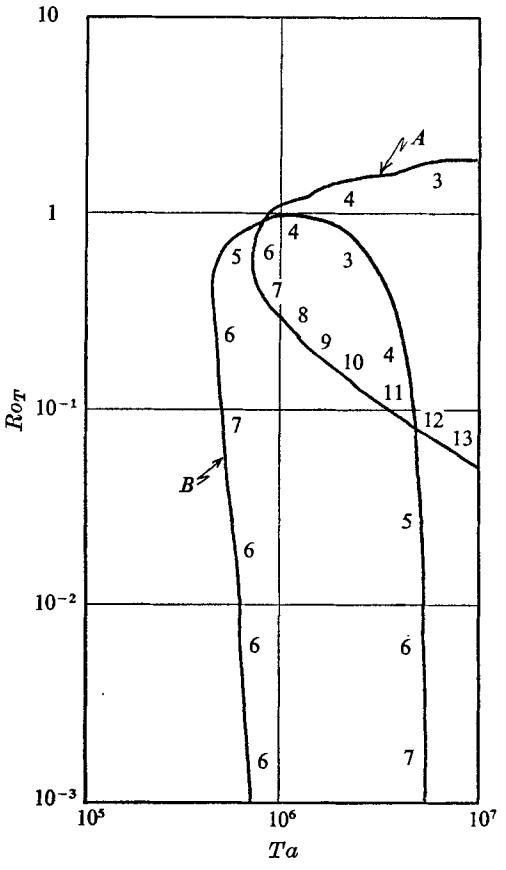

FIGURE 4. Marginal-stability envelopes based on the theory of baroclinic instability taking into account Ekman-layer friction at rigid upper and lower horizontal boundaries (curve A, Barcilon 1964) and also the slope of the geopotentials (curve B, Hide & Mason 1975; Mason 1976). The wavenumbers of the marginally stable waves are indicated against the curves. The imposed parameters correspond to the silicone-oil experiment (see figure 2) with $(\partial\rho/\partial r)/(\partial\rho/\partial z)$ taken as 0·5. The large differences between curves A and B show that the slope of the geopotentials plays a vital role in this area of parameter space, and the agreement between curve B, compared with curve A, and figure 2 is quite pronounced. In case B the wavenumbers of maximum instability are a maximum roughly half-way between the marginal-stability envelopes, and the value of this maximum is 12, 10 and 8 at $Ro_T = 10^{-3}$, 10^{-2} and 10^{-1} respectively. The cut-off in case B at $Ta \sim 5 \times 10^6$ is due to the geopotential slope becoming equal to the isotherm slope. The cut-off at $Ta \sim 5 \times 10^5$, the 'knee' of the regime diagram, is viscous in origin and appears to be in good agreement with the experiments. However, as noted by Douglas & Mason (1973), the quantitative agreement is fortuitous since there is a qualitative discrepancy between the depth-dependent friction parameter of the theory and the highly gap-width dependent experimental parameter Ta. In the case when the upper surface is free the theory no longer forms such a good model of the experiment. Calculations with two rigid surfaces only one of which slopes relative to the geopotential show effects akin to, though not quite so pronounced as, those when both slope relative to the geopotentials. (After the unpublished results of P. Mason.)

the regular wave regime. Similar maxima were observed for water (see Fein 1973) and mercury (see figure 8) as well as for water with a free upper surface (see Fein 1973).

As reported by others (e.g. Hide 1953, 1958), wavenumber determinations are subject to strong hysteresis effects. All transition points, and most experimental points within the regular wave regime, were approached from two directions in parameter space, by increasing as well as decreasing Ω along lines of constant ΔT. Different wavenumbers were observed at different times at the same point in parameter space. Generally, however, not more than two different wavenumbers were observed at any one point, and they were always consecutive.

The general character of the thermal wave patterns

Figures 5 and 6 show pen recordings of temperature as a continuous function of time measured at the mid-depth and mid-radius, at several discrete points along lines cutting across the regime diagram. Figure 5 represents a traverse along $\Delta T = 5{\cdot}00\,^{\circ}\mathrm{C}$ and figure 6 represents a vertical traverse at $\Omega = 6{\cdot}283\,\mathrm{rad/s}$ ($Ta = 2{\cdot}173 \times 10^6$). The time and amplitude scales are shown at the left of each trace segment. The 'cold' sides of the waves are the upper peaks. In both figures time progresses from right to left. The reader should be cautioned against judging the wave scale by the apparent scale of the thermal trace, which is a function not only of the wavelength but also of the drift rate of the thermal pattern and of the speed of the recording chart. The actual wavenumber is listed to the right of each thermal trace.

Along the traverse at $\Delta T = 5{\cdot}00\,^{\circ}\mathrm{C}$ (figure 5) the transition between upper symmetric flow and a steady (but slightly irregular) five-wave pattern clearly lies between $\Omega = 4{\cdot}189$ and $\Omega = 4{\cdot}331\,\mathrm{rad/s}$. No noticeable hysteresis effects were observed across the upper transition curve in experiments with a rigid lid in contact with the working fluid. The thermal wave amplitude is observed to increase in a linear fashion with increasing Ω and the wave patterns become progressively more regular and quasi-sinusoidal. At $\Omega = 6{\cdot}283\,\mathrm{rad/s}$, small-scale, low amplitude waves are observed superimposed on the basic, high amplitude, steady six-wave pattern. The wavenumber of the smaller-scale waves was found to be an odd multiple of six, but could not be determined beyond that. The drift rate of the smaller-scale waves was determined to be approximately twelve times greater than that of the steady six-wave pattern. At progressively higher rotation rates the basic six-wave pattern becomes progressivly less steady while the amplitudes of the smaller-scale waves grow. Moreover, the pattern of the smaller-scale waves becomes more complicated and is no longer identifiable as a simple multiple of six. Finally, at $\Omega = 7{\cdot}854\,\mathrm{rad/s}$ the wave pattern is judged to be characteristic of the irregular wave regime.

We concentrate next on figure 6, showing the traverse parallel to the Ro_T axis at $\Omega = 6{\cdot}283\,\mathrm{rad/s}$ ($Ta = 2{\cdot}173 \times 10^6$). The uppermost trace ($\Delta T = 30{\cdot}00\,^{\circ}\mathrm{C}$) is clearly irregular. The trace at $\Delta T = 10{\cdot}00\,^{\circ}\mathrm{C}$ represents a superposition of waves of wavenumber 6 and smaller-scale waves. At $\Delta T = 5{\cdot}00\,^{\circ}\mathrm{C}$ (the point of intersection of the two traverses) the six-wave pattern clearly dominates. At $\Delta T = 2{\cdot}40\,^{\circ}\mathrm{C}$ the synoptic pattern was found to consist of seven waves. The

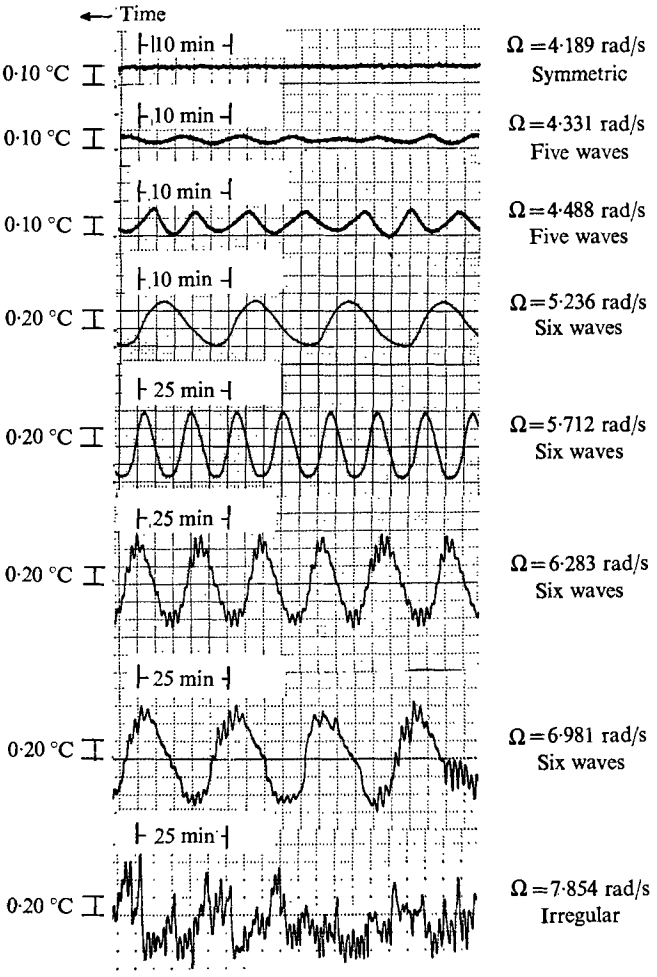

FIGURE 5. Temperature, as a continuous function of time, measured at mid-depth and mid-radius at discrete values of the rotation rate Ω along a traverse across the regime diagram for silicone oil ($Pr = 63$) at $\Delta T = 5{\cdot}00$ °C. Time progresses from right to left. The cold sides of the waves are the upper peaks. The time and temperature scales are shown to the left of each thermal pattern.

choppy appearance of the trace of temperature *vs.* time is believed to be due to the very slow drift of the pattern. At values of ΔT less than 2·40 °C the drift rates were observed to be extremely small and it was necessary to use the rotating probe in order to traverse the remainder of the regime diagram within a reasonable period of time. The probe made a complete circuit around the annulus in one hour. The irregular features evident at low values of ΔT (in particular at $\Delta T = 1{\cdot}00$ °C) repeated themselves essentially without change at every revolution of the probe. Similar irregularities were observed in water (see Fein 1973) at low values of ΔT. For the purpose of comparison, measurements with both the rotating and the stationary probe were made at $\Delta T = 0{\cdot}15$ °C and are shown in figure 6.

In silicone oil transient times were generally quite short. Steady-state conditions were usually attained in just a few minutes (one or two wave periods),

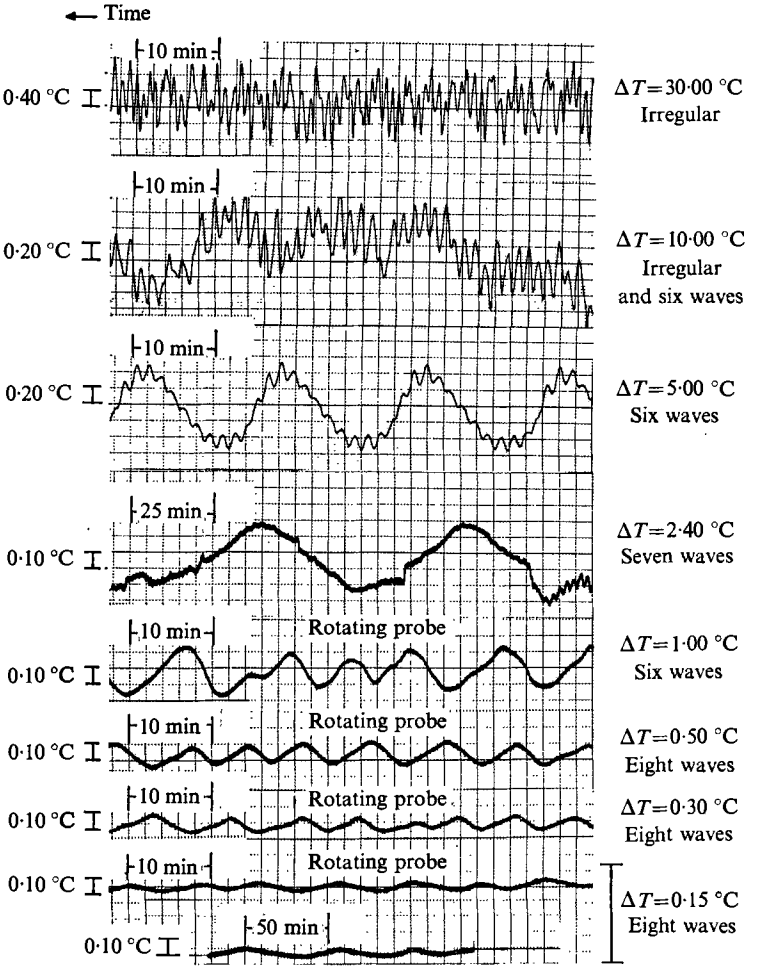

FIGURE 6. Temperature, as a continuous function of time, measured at mid-depth and mid-radius at discrete values of ΔT along a traverse across the regime diagram for silicone oil ($Pr = 63$) at $\Omega = 6{\cdot}283$ rad/s ($Ta = 2{\cdot}173 \times 10^6$). Time progresses from right to left. The cold sides of the waves are the upper peaks. The time and temperature scales are shown to the left of each thermal pattern.

except at points in the regime diagram near the transition to irregular waves, at which small-scale structure was superimposed upon the basic large-scale pattern (e.g. at $\Delta T = 5{\cdot}00\,°\mathrm{C}$, $\Omega = 6{\cdot}283$ rad/s; figures 5 and 6). At such points slight changes in the wave pattern were observed over several tens of minutes before a steady state was attained.

The thermal wave amplitude

At different constant values of ΔT the thermal wave amplitudes in silicone oil were found to increase linearly with decreasing rotation period $2\pi/\Omega$. This behaviour is qualitatively similar to that for water (with a rigid upper boundary) in the vicinity of the upper transition curve. While the amplitudes of the fully developed thermal waves were approximately 50 % greater in water than they

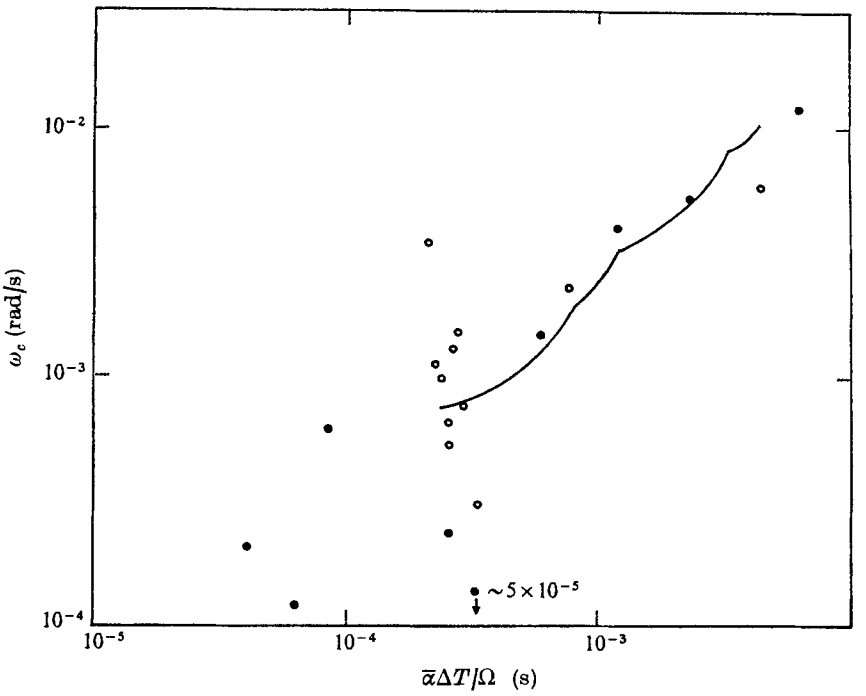

FIGURE 7. The thermal wave pattern's angular drift rate ω_c at transitions from the symmetric to the regular wave regime as a function of the imposed thermal wind $\bar{\alpha}\Delta T/\Omega$ for water (Pr = 7·16, solid curve, after Fein 1973), silicone oil (Pr = 63, solid circles) and mercury (Pr = 0·0246, open circles).

were in silicone oil, the magnitudes of the slopes of the curves of thermal wave amplitude *vs.* $2\pi/\Omega$ were larger in silicone oil, particularly at low values of ΔT (cf. Fein 1973, figures 11 and 12).

Wave drift

Figure 7 shows the angular drift velocity ω_c of the thermal wave pattern as a function of the imposed thermal 'wind' $\bar{\alpha}\Delta T/\Omega$ along the transition curve between the upper symmetric regime and the regular wave regime. The solid curve, closed circles and open circles are for water (after Fein 1973), silicone oil and mercury, respectively. At values of $\omega_c \geqslant 10^{-3}$, which correspond to measurements at $\Delta T \geqslant 2{\cdot}40\,^{\circ}\mathrm{C}$, the data for silicone oil lie near the curve for water. At values of $\omega_c < 10^{-3}$ the data show considerable scatter. In the latter region the wave drift periods were so great that it was usually feasible to record the passage of only a single wave train. Measured drift periods often varied by a factor of several tenths and the experimental uncertainties in attempting to measure and maintain the small temperature differences ΔT were often as high as 50%. Within the regular wave regime the drift rates ω were quite close to those shown for the transition points (ω_c), with the bulk of the data points lying slightly to the right of and below those shown in figure 7. The same behaviour was observed in the case of water (Fein 1973), where there was also considerable scatter of the data points at $\omega < 10^{-3}$.

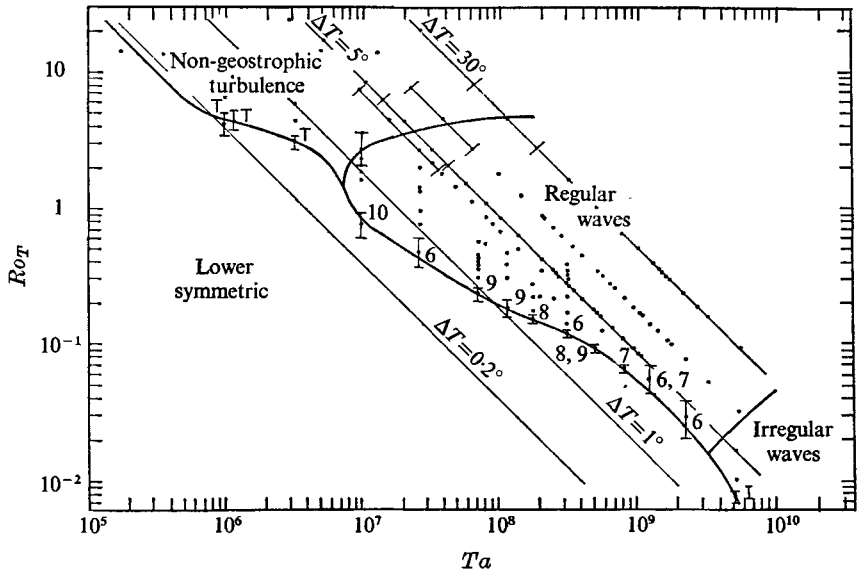

FIGURE 8. The regime diagram for mercury (Pr = 0·0246). The circles within the regular wave regime are experimental points at which the thermal wavenumber, amplitude and angular drift rate were measured. Experimental conditions: $b-a$ = 2·54 cm, d = 5·00 cm, $\bar{T}$ = 20·00 °C, $\bar{\nu}$ = 1·14 × 10^{-3} cm²/s, $\bar{\rho}$ = 13·546 g/cm³, Pr = 0·0246, upper surface rigid.

5. Results for mercury (Pr = 0·0246)

The regime diagram

Figure 8 shows the regime diagram for mercury plotted in log–log co-ordinates in dimensionless two-parameter space (Ro_T *vs.* Ta). The regular wave regime in mercury is displaced towards higher values of the Taylor and thermal Rossby number by approximately an order of magnitude along each axis relative to its position on the diagram for water. The shape of the transition curve separating the lower symmetric regime from the regular wave regime is quite similar to that for water (see Fein 1973), being only weakly dependent upon the rotation rate, with average slopes of about $-\frac{1}{2}$ in the range of Taylor numbers $10^7 \leqslant Ta \leqslant 10^8$ and -1 around $Ta \sim 10^9$. The transitions along this curve were generally sharp and free of hysteresis, and the wave amplitude was observed to increase linearly as ΔT was increased beyond $(\Delta T)_c$.

A notable feature of the regime diagram for mercury is the absence of an upper symmetric regime and the presence of a turbulent regime at high values of the thermal Rossby number within the range of Taylor numbers surveyed. In this portion of dimensionless parameter space the Reynolds numbers with respect to the probe and with respect to the annular gap width were large (approximately 100 and 2500, respectively, at $Ro_T \sim 5$, $Ta \sim 5 \times 10^7$) and the Richardson number was low ($Ri \sim 1$). The transitions between the turbulent regime and the lower symmetric regime were sharp and were free of hysteresis effects, whereas the transitions between the turbulent regime and the regular wave regime took place

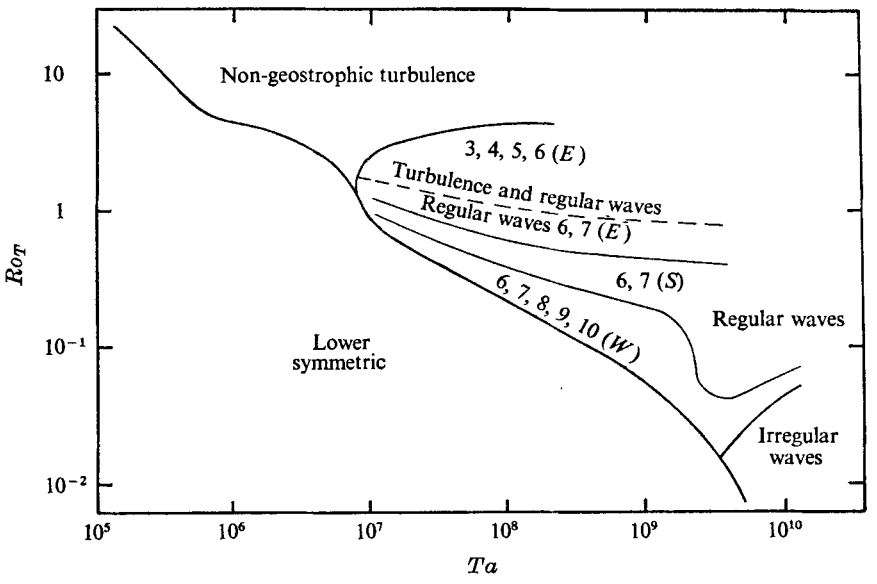

FIGURE 9. The general character of the convection within the wave regime for mercury (Pr = 0·0246) in terms of regular and irregular wave patterns, wavenumbers and wave drift directions. E, easterly drift (from east to west or anti-rotation); W, westerly drift (from west to east or pro-rotation); S, stationary, or standing waves.

over a broad zone which was characterized by turbulence superimposed upon baroclinic-scale waves ($3 \leqslant N \leqslant 6$).

Accurate measurements were difficult to make at very high rotation rates and only a few such measurements were attempted at moderate and low values of ΔT. The results (e.g. the temperature trace at the bottom of figure 12) strongly suggest the presence of a transition between the regular and an irregular wave regime at $Ta \sim 5 \times 10^9$ in the vicinity of the lower transition curve, shifting towards higher Taylor numbers as the thermal Rossby number is increased. This is consistent with the results for water and for silicone oil.

The wavenumber regimes

A broad spectrum of wave characteristics was observed within the regular wave regime. These are summarized in figure 9. The transition zone of wavenumbers 3–6 with superimposed turbulence extends below $Ro_T \sim 1$. The waves in this zone drifted from 'east' to 'west'. As Ro_T was decreased the turbulence disappeared and the wave patterns became more regular in appearance with a wavenumber of either 6 or 7 dominating. Easterly waves changed into stationary waves and finally into westerly waves as Ro_T was decreased further towards the lower symmetric regime. The highest wavenumbers and the most regular wave patterns were observed near the lower transition curve. At very low values of Ro_T and high values of Ta the regular wave patterns gave way to irregular time-dependent wave patterns which resembled those in the irregular wave regimes for water and for silicone oil.

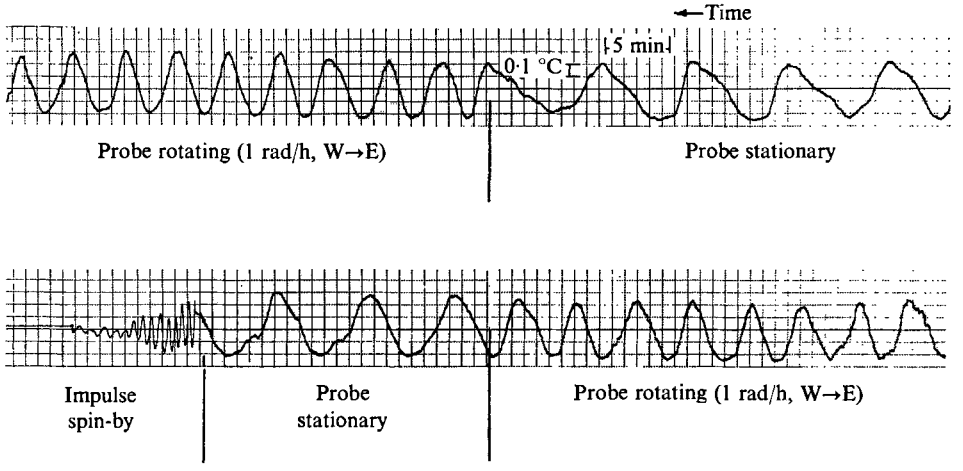

FIGURE 10. An example of 'easterly' waves ('westward' wave drift) in mercury (see text for explanation).

The general characteristics of the thermal wave patterns

In order to determine the direction in which a pattern drifted it was necessary to use both rotating and stationary probes. Figure 10 shows an example of such a determination. The experimental conditions here are $\Delta T = 2{\cdot}50\,^{\circ}\mathrm{C}$ and $\Omega = 0{\cdot}758\,\mathrm{rad/s}$, corresponding to $Ro_T = 0{\cdot}558$ and $Ta = 7{\cdot}90 \times 10^7$. The wave patterns at this particular point in parameter space drifted from 'east' to 'west', or counter-rotated.

The time and amplitude scales were constant and are shown at the upper right. (The total length of time for the 'impulse spin-by' trace was approximately 25 s.) The traces shown were continuous in time, from right to left and top to bottom. The 'impulse spin-by' of the wave pattern past the stationary probe (shown at the lower left) was at an initial speed of approximately 3 cm/s.

The first 30 min of the experiment are depicted by the trace at the upper right. During that period five waves drifted past the stationary probe (ten waves per hour). The probe was then set in motion from 'west' to 'east' round the annulus at 1 rev/h. After a period of one hour sixteen waves were recorded. If a number N of waves less than 10 had been recorded by the rotating probe then the pattern would have been $10-N$ waves drifting from 'west' to 'east'. For $N > 10$ the pattern would have been $N-10$ waves drifting from 'east' to 'west'. Therefore the pattern measured was six waves drifting against the rotation, or 'east' to 'west'.

The probe was made stationary again (lower left) to check for hysteresis, which was not evident, and, finally, the annulus was impulsively spun up in order to obtain an independent wavenumber measurement, which, as it turned out, was also six.

Because of the wide range of wave characteristics within the wave regime for mercury, we shall show thermal wave patterns along four traverses through that regime. Two were at 45° to the axis along the lines $\Delta T = 30{\cdot}00\,^{\circ}\mathrm{C}$ and $\Delta T = 5{\cdot}00\,^{\circ}\mathrm{C}$ and are shown in figures 11 and 12, respectively, and two were vertical traverses parallel to the Ro_T axis at $Ta = 9{\cdot}560 \times 10^6$ ($\Omega = 0{\cdot}273\,\mathrm{rad/s}$)

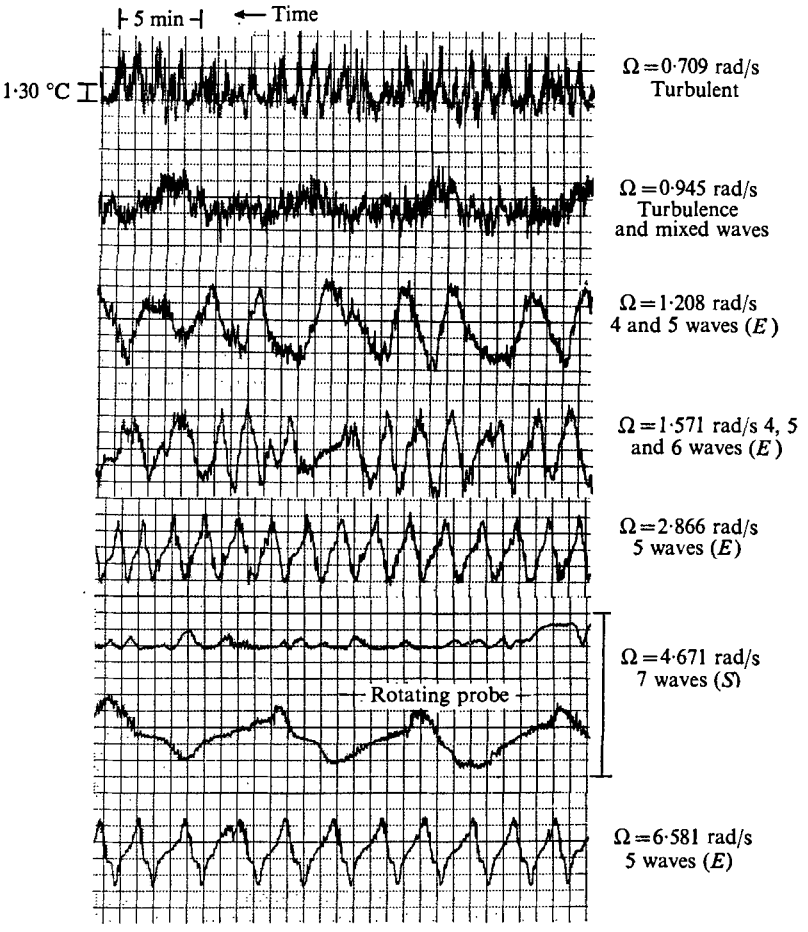

FIGURE 11. Temperature, as a continuous function of time, measured at mid-depth and mid-radius at discrete values of the rotation rate Ω along a traverse across the regime diagram for mercury (Pr = 0·0246) at ΔT = 30·00 °C. Time progresses from right to left. The cold sides of the patterns are the upper peaks. The time and temperature scales are shown at the upper left.

and $Ta = 3{\cdot}161 \times 10^8$ (Ω = 1·571 rad/s) and are shown in figures 13 and 14, respectively.

All the thermal patterns shown along these traverses were measured at the mid-radius and mid-depth. The amplitude and time scales are shown at the left of the trace segments. When these scales were constant they are shown but once, at the upper trace. Time progresses from right to left and the cold sides of the waves are the upper peaks. When the rotating probe (1 rev/h) was used this is indicated to the right of the trace segment.

Concentrating first on the traverse at ΔT = 30·00 °C shown in figure 11 we see that the transition from fully turbulent flow (at Ω = 0·709 rad/s) to predominately baroclinic (large) scale flow (at Ω = 1·208 rad/s) was gradual. The wave patterns observed at intermediate values of Ω (e.g. at Ω = 0·945 rad/s) were characterized by strong turbulence superimposed on baroclinic-scale waves. As

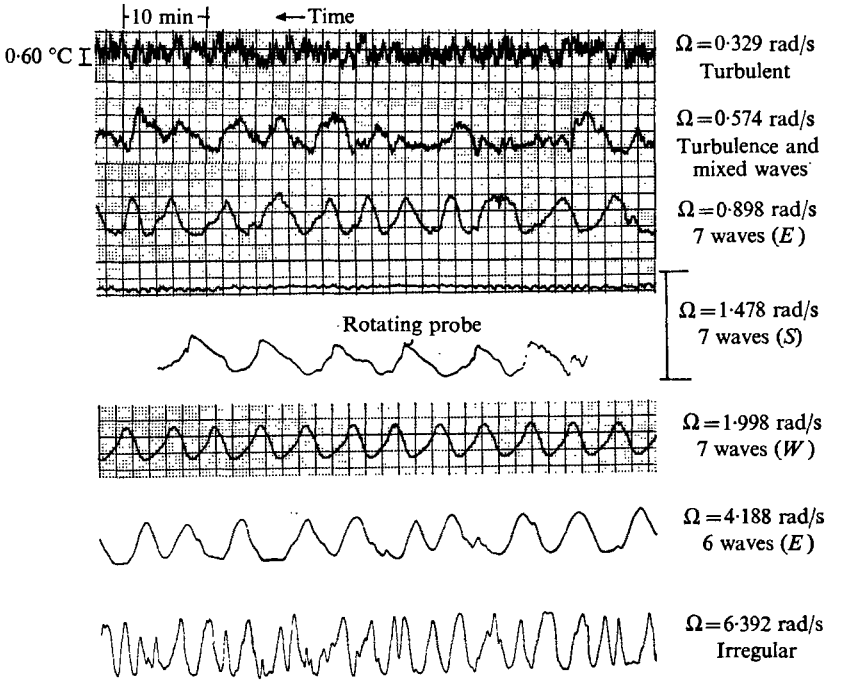

FIGURE 12. Same as figure 11 except $\Delta T = 5{\cdot}00$ °C.

Ω was increased, progressing into the regular wave regime, the amplitude of the turbulence decreased. However, it remained finite even at relatively large values of Ω deep within the wave regime. (This was not the case at lower values of ΔT as we shall see below when we discuss the traverse at $\Delta T = 5{\cdot}00$ °C.) Also, as Ω was increased, the wave patterns became more regular. The major large-scale irregularities shown at $\Omega \leqslant 1{\cdot}571$ rad/s as well as the minor irregularities in the traces shown for $\Omega \geqslant 2{\cdot}866$ rad/s were time dependent. That is, they did not repeat in any regular fashion.

At high values of ΔT (and $Ta \leqslant 10^{10}$) the waves were observed to drift either from 'east' to 'west' or not at all. The wave pattern at $\Omega = 4{\cdot}671$ rad/s was stationary, and at that point both the stationary and rotating probe measurements are shown.

The traverse at $\Delta T = 5{\cdot}00$ °C shown in figure 12 shows some additional variety in terms of wave characteristics. The transition from turbulent to wavelike flow is again seen to be gradual. However, all signs of turbulence disappear at rotation rates not very far into the regular wave regime. At low values of Ω the seven-wave pattern drifted from 'east' to 'west'. As Ω was increased it became stationary and fairly regular. A further increase of Ω to 1·998 rad/s resulted in a very regular, steady, seven-wave pattern which drifted from 'west' to 'east'. This regularity, however, soon gave way to progressively less regular waves as Ω was increased through 4·188 rad/s. Beyond this value of Ω the patterns were quite irregular and time dependent and the waves were observed to drift once again from 'east' to 'west'.

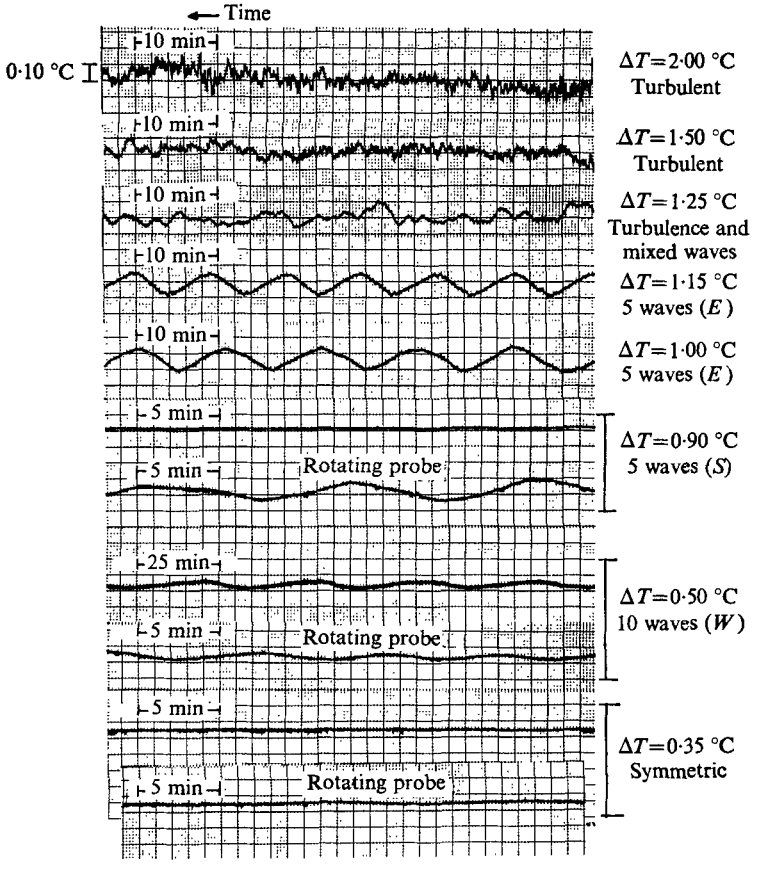

FIGURE 13. Temperature, as a continuous function of time, measured at mid-depth and mid-radius at discrete values of the imposed horizontal temperature gradient ΔT along a traverse across the regime diagram for mercury (Pr = 0·0246) at Ω = 0·273 rad/s ($Ta = 9{\cdot}560 \times 10^6$). Time progresses from right to left. The cold sides of the patterns are the upper peaks. The time and temperature scales are shown at the left.

Along this particular traverse at ΔT = 5·00 °C static-stability measurements were made at fairly close intervals of Ω. These will be discussed in a section to follow. The reader might find it worthwhile at this point, however, to glance at figure 16. The patterns shown in that figure fill some of the gaps in figure 12 and a clearer picture of the various characteristics of the regular wave regime may be obtained by studying it.

The vertical traverse through the 'knee' of the regime diagram at $Ta = 9{\cdot}560 \times 10^6$, shown in figure 13, depicts a transition from the lower symmetric to the regular wave regime as well as from the regular wave regime to the non-geostrophic turbulent regime. At the lower transition a steady ten-wave pattern was observed which drifted very slowly from 'west' to 'east'. As ΔT was increased to 0·90 °C, a steady stationary five-wave pattern developed. Further increasing ΔT, by only 10 %, to 1·00 °C, resulted in the steady five-wave pattern drifting from 'east' to 'west' with a moderate drift period of approximately 10 min. The changes in thermal amplitude, as a function of ΔT, were regular and

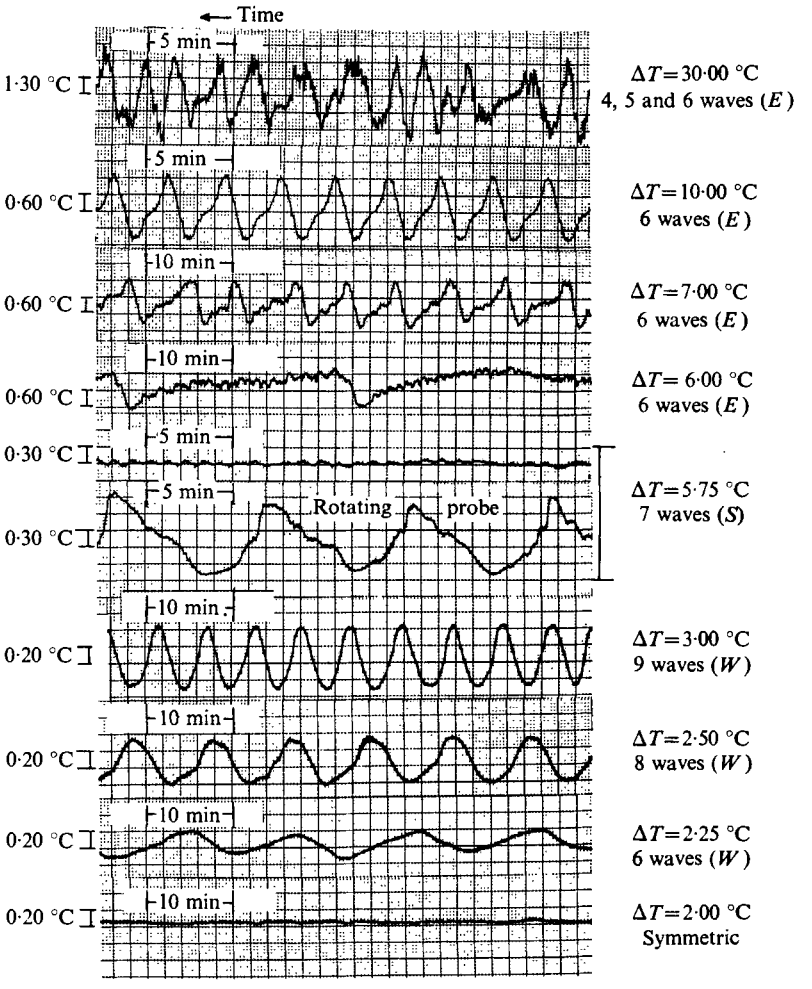

FIGURE 14. Same as figure 13 except $\Omega = 1{\cdot}571$ rad/s ($Ta = 3{\cdot}16 \times 10^8$).

quasi-linear through this value of ΔT. The transition to non-geostrophic turbulent flow occurred somewhere in the range $1{\cdot}15\,°\text{C} < \Delta T < 1{\cdot}50\,°\text{C}$.

The last traverse to be discussed was again a vertical traverse, but well within the regular wave regime at $Ta = 3{\cdot}161 \times 10^8$ (figure 14). The transition from the lower symmetric to the regular wave regime was similar in character to that shown in the previous figure at $Ta \sim 10^7$. The changes in wave amplitude, as a function of ΔT, were regular and fairly linear. The wave patterns in the vicinity of the lower transition curve (i.e. $2{\cdot}25\,°\text{C} < \Delta T < 3{\cdot}00\,°\text{C}$) were characterized by relatively large wavenumbers, very regular steady features and pro-rotation drift directions, i.e. 'west' to 'east'. As ΔT was increased, (i) the wavenumbers decreased slightly, (ii) the wave patterns ceased drifting at $\Delta T = 5{\cdot}75\,°\text{C}$ and drifted from 'east' to 'west' at higher values of ΔT, and (iii) the patterns became progressively less regular until, finally, at $\Delta T = 30{\cdot}00\,°\text{C}$ weak turbulence superimposed upon an irregular baroclinic-scale pattern of wavenumbers 4–6 was observed.

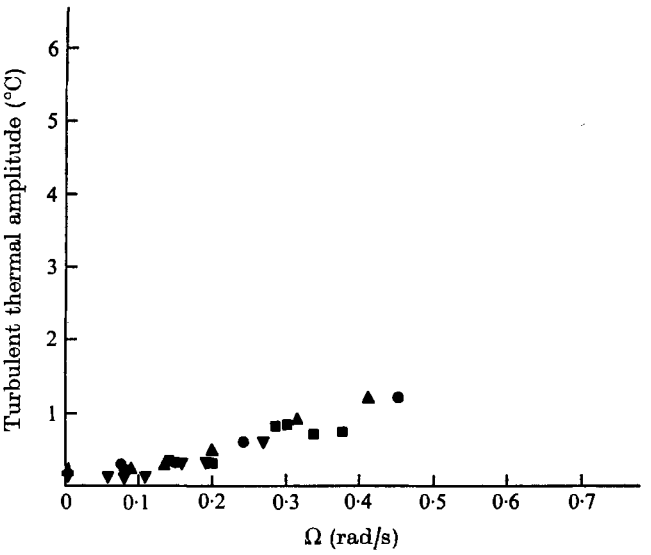

FIGURE 15. Thermal amplitude of the turbulent convection in mercury (Pr = 0·0246) as a function of the rotation rate Ω along traverses through the non-geostrophic turbulent regime at several values of ΔT: ●, 30·00 °C; ▲, 10·00 °C; ■, 5·00 °C; ▼, 4·00 °C.

Over large regions of parameter space transient times in mercury were difficult to assess because of the general unsteadiness of the flow. The reader should keep this in mind with respect to the information which follows. For lower transitions, a steady state was usually reached in about 10 min. Within the regular wave regime, for changes in ΔT of about 15 % a steady state was reached in about 5 min. For several isolated cases, within the regular wave regime, when regular waves developed from transients composed of a baroclinic-scale wave pattern and superimposed turbulence, a steady state was reached in approximately 1 h.

The thermal wave amplitudes

The wave patterns in the vicinity of the transition to turbulence were characterized by the superposition of baroclinic and turbulent scales. No attempt was made to separate these components. Therefore no information was obtained regarding the amplitude of the baroclinic modes as a function of parameter space near that transition.

Within the non-geostrophic turbulent regime, however, the thermal amplitude decreased monotonically as Ω was decreased. Moreover, it was observed to be nearly independent of ΔT. This result is shown schematically in figure 15, which is a plot of the thermal amplitude of the turbulence, as a function of Ω, along traverses at ΔT = 30·00, 10·00, 5·00 and 4·00 °C.

The thermal wave amplitude in the vicinity of the lower transition was observed to vary directly with ΔT in a regular manner similar to that observed for water (cf. Fein 1973). The magnitude of the changes in amplitude, with respect to ΔT, increased as Ta was increased. Near the 'knee', where the growth was slow, the amplitude increased by approximately 30 % of increases in ΔT (see

figure 13). At large values of Ta the amplitude increased by about the same amount as ΔT was increased (see figure 14).

The amplitudes of the fully developed thermal waves within the regular wave regime for mercury were comparable to those observed in water by Fein (1973).

The thermal wave drift characteristics

One of the least regular phenomena observed in this study was the drift characteristics of the waves in mercury. Within the wave regime the magnitude as well as the sense of the drift varied very rapidly as a function of ΔT and Ω. In figure 9 we indicated where in the wave regime 'easterly', 'westerly' and stationary waves were observed. Outside the stationary regime and away from the immediate vicinity of its boundaries typical periods for a wave train to travel completely round the annulus were approximately 15 and 30 min at $\Delta T = 30{\cdot}00$ and $5{\cdot}00\,^{\circ}\mathrm{C}$ respectively. In general the period was observed to lengthen with decreasing values of ΔT and increasing values of Ω. However no regularity was evident. In terms of normalized drift periods, at $Ta \sim 5 \times 10^8$ (approximately midway across the regular wave regime) a wave train drifted round the annulus in approximately 200 and 700 rotation periods Ω^{-1} at $\Delta T = 30{\cdot}00\,^{\circ}\mathrm{C}$ ($Ro_T \sim 1$) and $\Delta T = 5{\cdot}00\,^{\circ}\mathrm{C}$ ($Ro_T \sim 0{\cdot}2$) respectively. The drift was from 'east' to 'west' in the former case and from 'west' to 'east' in the latter.

The only quantitative results we shall show are drift data at lower transitions, which, by the way, were nearly as non-regular. These are plotted in figure 7 along with ω_c at the upper transition for silicone oil and water. Two data points were in reasonably close agreement with the nearly linear dependence upon the imposed thermal wind exhibited by the water and silicone-oil data. However, most of the mercury data fell along the line $\bar{\alpha}\Delta T/\Omega \sim 3 \times 10^{-4}$. A substantial portion of the lower transition curve for mercury sloped towards larger values of ΔT as Ta increased (see figure 8). As it turned out, along that portion of the curve lower transitions occurred at a nearly fixed value of the imposed thermal wind, and at that value ω_c varied by approximately an order of magnitude centred about a value of about 10^{-3}.

6. Some gross features of the vertical thermal structure as a function of the Prandtl number

Because of several unique features of the regime diagrams for silicone oil and mercury, in particular, the absence of an upper symmetric regime and the existence of a non-geostrophic turbulent regime for mercury and the absence of a lower symmetric regime for silicone oil, it was decided to measure the static stability in all three fluids on traverses along the isotherm $\Delta T = 5{\cdot}00\,^{\circ}\mathrm{C}$. The objective was to gather data on the internal thermal structure, which, it was anticipated, might illuminate the dynamical processes which controlled the preferred existence of one mode of convection over another, as a function of the Prandtl number.

Temperature measurements were made simultaneously at the mid-radius at two levels, $d = 0{\cdot}40$ (T_1) and $d = 4{\cdot}60\,\mathrm{cm}$ (T_3), which were chosen to correspond to levels in the interior of the fluid just above the lower Ekman layer and just

below the upper Ekman layer. The temperature difference $\Delta_z T$ ($= T_3 - T_1$) was computed at approximately ten equally spaced intervals along the wave as it drifted past the two stationary probes. The average of these values, the zonal mean† static stability $\overline{\Delta_z T}$, was then computed.

In silicone oil and water, measurements were made in the upper symmetric regime, across the upper transition, and into the fully developed regular wave regime. In mercury, measurements were made in the non-geostrophic turbulent regime, within the region of transition between turbulent and wave flow, and within the regular wave regime. All points in parameter space at which static-stability measurements were made correspond to data points at which mid-depth measurements of the thermal wavenumber, amplitude and drift rate had previously been made.

The zonal mean static stabilities in silicone oil and water were very similar. $\overline{\Delta_z T}$ was approximately 3° C in water and just a few per cent higher in silicone oil. Moreover, it varied very little, as a function of Ω, along the traverse at $\Delta T = 5{\cdot}00$ °C (which extended approximately an order of magnitude in Ta). In particular, at the upper transition, no sharp changes were observed. In fact, in terms of static-stability changes, these transitions were indistinguishable from changes in other regions of parameter space. In both fluids the thermal profiles were convective, i.e. within the interior of the fluid the slope of the isothermal surfaces was somewhat less than unity.

By contrast, in mercury the zonal mean static stability $\overline{\Delta_z T}$ varied strongly as a function of Ω, increasing from zero within the regular wave regime, at $Ta \geqslant 10^8$, to approximately 1 °C within the non-geostrophic turbulent regime, at $Ta \sim 10^7$ (see figure 18). No unusual changes were observed in the region of transition to turbulence. Hence the thermal profile in mercury was purely conductive deep within the regular wave regime and essentially conductive within the non-geostrophic turbulent regime (at least over the range of parameter space surveyed: $Ro_T \lesssim 10$, $Ta \gtrsim 10^7$), where the isothermal slope deviated from the vertical by less than 20°.

In silicone oil and water, thermal wave amplitudes were a maximum at the mid-depth, a minimum just below the upper Ekman layer, at 4·60 cm, and intermediate just above the lower Ekman layer, at 0·40 cm. The distribution of the zonal mean temperature in both fluids was asymmetric. That is, the zonal mean temperature $\overline{T}_2$ measured at the mid-depth and mid-radius was approximately 21 °C in water and slightly greater in silicone oil. A symmetric distribution would have required $\overline{T}_2 = \overline{T} = 20{\cdot}00$ °C. This observation implied that an intense cold pocket of fluid was confined to the lower levels of the annulus with strong thermal gradients in those regions.

In mercury the thermal amplitude of the wave patterns was observed to be only weakly dependent upon depth. That is, at all three levels at which waves

† For steady waves, time and space intervals were related by the constant drift rate of the wave pattern. Measurements made at one point in space at different times would have been identical to measurements made at one time at different azimuthal points along the wave. This was not true for unsteady and turbulent patterns, as were observed in mercury. For those cases, the 'zonal mean' was actually a combined zonal and temporal mean.

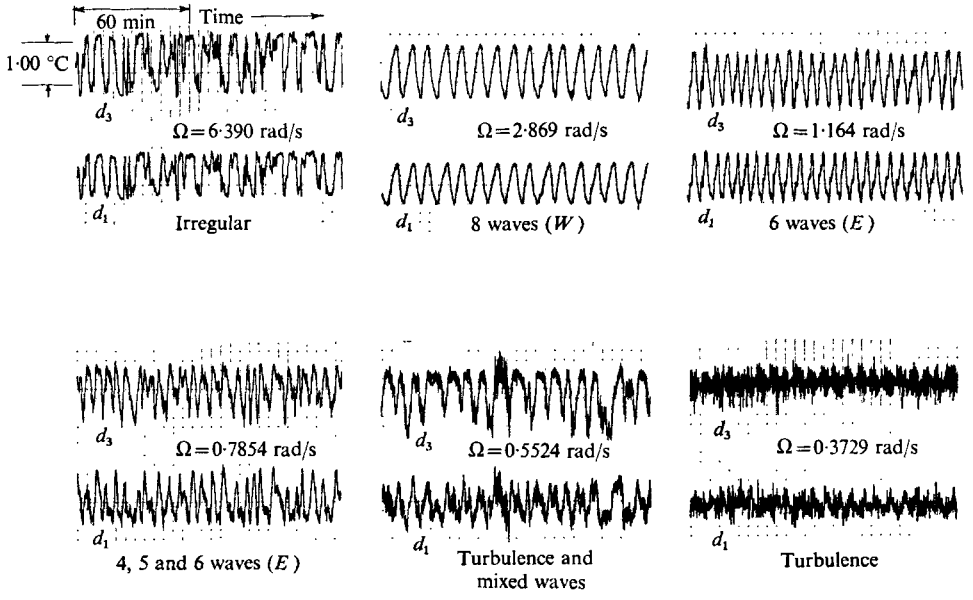

FIGURE 16. Temperature, as a continuous function of time, measured simultaneously at mid-radius and two depths (d = 0·40 and d_3 = 4·60 cm) at discrete values of the rotation rate Ω along a traverse across the regime diagram for mercury (Pr = 0·0246) at ΔT = 5·00 °C. Time progresses from left to right. The warm sides of the patterns are the upper peaks. The time and temperature scales are shown at the upper left thermal pattern.

were observed their amplitudes were of nearly equal magnitude. Approaching the transition region to turbulent flow, within that region, and in the fully developed non-geostrophic turbulent regime, the thermal amplitude at the mid-depth was approximately 20 and 50 % less than those at 0·40 cm and 4·60 cm respectively.

As observed for silicone oil and water, the mean temperatures at the mid-depth in mercury were nearly 1 °C higher than the overall imposed mean temperature of the fluid. Since the static stability in mercury was small, this implied intense gradients of cold fluid along the inner wall of the annulus.

In all three fluids the thermal wave patterns were perfectly correlated in the vertical. No significant differences were evident between the phases of the (baroclinic scale) thermal waves at depths of 0·40 and 4·60 cm. An exception was observed, however, approaching and within the non-geostrophic turbulent regime in mercury, where the correlation was less perfect, and became progressively worse as Ro_T was increased. This can be seen in figure 16, which shows a selected number of thermal wave patterns in mercury, along the traverse at ΔT = 5·00 °C, measured simultaneously at depths d_1 = 0·40 cm and d_3 = 4·60 cm. At high values of Ω, deep within the regular wave regime, the wave phases at d = 0·40 and 4·60 cm were perfectly correlated. This was true not only with respect to the largest scales but also with respect to minor irregularities. This was particularly obvious at Ω = 6·390 rad/s, but can be seen also at lower values of Ω. At Ω = 0·7854 rad/s (in the wave regime close to the zone of transition to turbulence), the correlation was much less perfect and became progressivly worse as the rotation rate was decreased and the convection became more turbulent.

In figure 17 thermal wave patterns in silicone oil, water and mercury are shown at $d = 0{\cdot}40$, $2{\cdot}50$ and $4{\cdot}60$ cm. Those at $0{\cdot}40$ and $4{\cdot}60$ cm were measured simultaneously. Those at $2{\cdot}50$ cm were obtained from previous experiments. For all three fluids the patterns shown correspond to points in parameter space within the fully developed regular wave regime. The amplitude scales are constant and are shown along the right edge of the figure. The time scales are identical for silicone oil and water but differ by a factor of two for mercury as shown at the lower right. Time progresses right to left and the cold sides of the waves are the upper peaks.

Plotted alongside the thermal wave traces are subjective analyses of the zonal mean thermal structure (plotted in a meridional cross-section) in each fluid. These analyses are based *only* on measurements made at the mid-radius and are marked by the three triangles. For each fluid, zonal mean temperatures were deduced at each of the six points marked by solid circles. These points were chosen at distances of $0{\cdot}40$ cm from the side walls, where it was assumed they would be in the interior of the fluid, just outside the thermal boundary layers.

The temperature at each of those points was obtained by assuming that the thermal wave amplitude measured at the mid-radius was a good measure of the interior horizontal temperature difference $\Delta_r T$.† Thus the zonal mean temperature near the hot wall was taken to be the maximum temperature of the wave which was measured at the mid-radius, and that near the cold wall the minimum. This procedure was applied at each depth. Combined with zonal mean temperature measurements at the mid-radius at each depth, this yielded three measured (triangles) and six deduced (circles) zonal mean temperatures. On the basis of these, the meridional profiles shown in figure 17 were drawn.

The right wall of the annulus schematically drawn in that figure is the hot wall, which was maintained at $22{\cdot}50\,^{\circ}$C. The left wall is the cold wall, maintained at $17{\cdot}50\,^{\circ}$C. The isotherms are drawn at $0{\cdot}50\,^{\circ}$C intervals.

Because of the many assumptions upon which these profiles are based, the reader is cautioned against taking them too literally. One outstanding feature, however, is most certainly real. For fully developed waves in silicone oil and water the interior thermal field is convective, i.e. in the heat equation the nonlinear, convective terms dominate. For comparatively fully developed waves in mercury, however, the interior thermal field is strongly conductive, i.e. in the heat equation the linear conduction term $\bar{\kappa}\nabla^2 T$ dominates.

As we have already pointed out for mercury, as the rotation rate was decreased the static stability slowly increased. This is depicted schematically in figure 18, in which the thermal patterns and zonal mean thermal structures are shown for mercury at $\Delta T = 5{\cdot}00\,^{\circ}$C and $\Omega = 1{\cdot}995$, $0{\cdot}9023$ and $0{\cdot}5026$ rad/s. At these values of the rotation rate, $\overline{\Delta_z T}$ was 0, $0{\cdot}4$ and $0{\cdot}7\,^{\circ}$C respectively. The description of the construction of the thermal profiles which were shown in figure 17 also applies

† This assumption was based upon multi-probe measurements of synoptic thermal fields in glycerol/water solutions made at the Geophysical Fluid Dynamics Institute, Florida State University, Tallahassee. Those measurements indicated that, within the fully developed wave regime, the thermal wave amplitude was equal to the interior horizontal temperature gradient to within 10%.

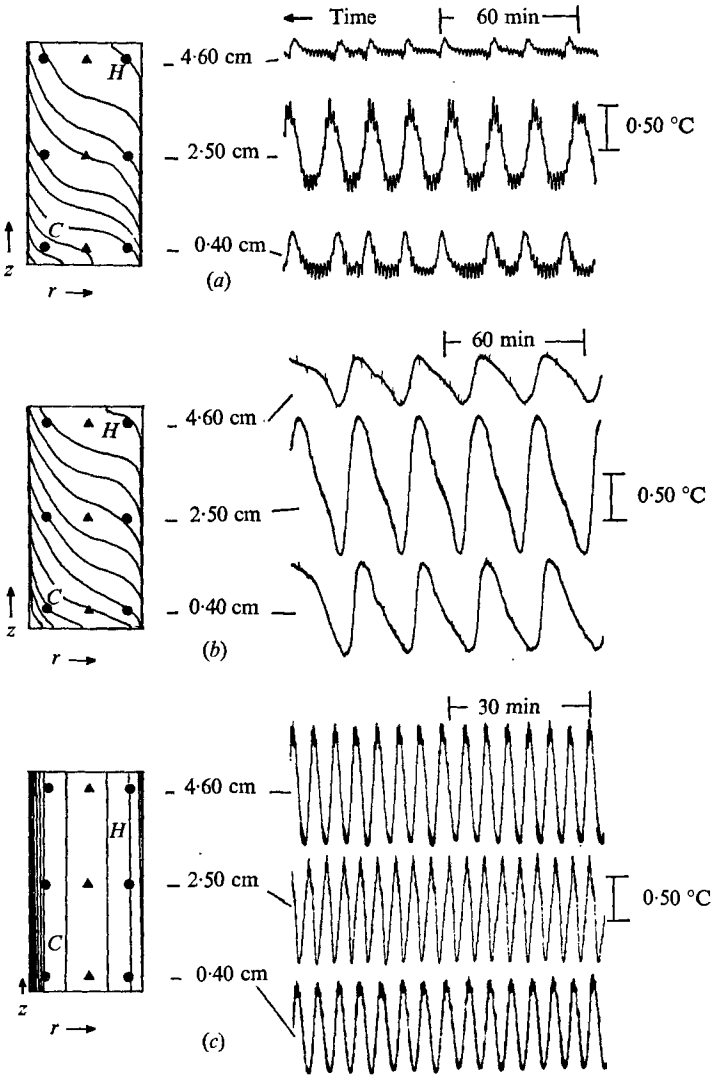

FIGURE 17. Temperature, as a continuous function of time, measured at mid-radius and three depths (0·40, 2·50 and 4·60 cm) within the fully developed wave regimes of (*a*) silicone oil, (*b*) water and (*c*) mercury at $\Delta T = 5{\cdot}00$ °C. The measurements at 0·40 and 4·60 cm were made simultaneously. Those at 2·50 cm are reproduced from previous experiments. Time progresses from right to left. The cold sides of the waves are the upper peaks. The time and temperature scales are shown at the right of the thermal patterns. (Note that the time scale for the measurements in mercury differs from the others by a factor of two.) To the left of the thermal patterns are *highly subjective* sketches of the meridional temperature profiles. They were each based upon only three measured zonally averaged temperatures (marked by the triangles in the meridional plane), which correspond to the mean temperatures of the wave patterns shown at the right. Zonally averaged temperatures were *deduced* at six additional points in the meridional plane marked by the circles (see text for details).

	Pr	Ω	Ro_T	Ta	Number of waves
(*a*)	63	6·283	0·101	$2{\cdot}17 \times 10^6$	6
(*b*)	7·16	2·244	0·155	$8{\cdot}22 \times 10^6$	6
(*c*)	0·0246	1·995	0·173	$5{\cdot}10 \times 10^8$	7 (W)

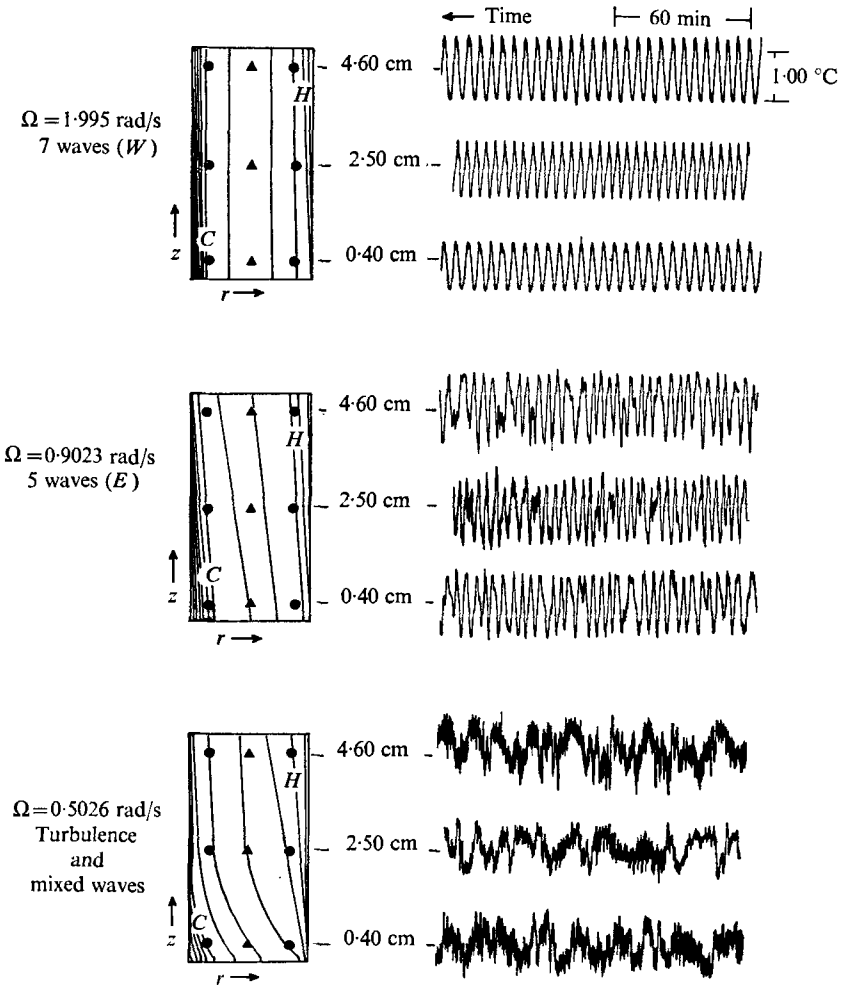

FIGURE 18. Same as figure 17 except that all data are for mercury at the three values of the rotation rate Ω indicated along a traverse across the regime diagram at $\Delta T = 5{\cdot}00$ °C, with different wave patterns as marked.

to this figure. The important feature to note in figure 18 is the very mild overturning of the isothermal surfaces as Ω was decreased. Even at relatively low values of Ω, within the non-geostrophic turbulent regime, the thermal profile was still highly conductive.

Although knowledge of the field of static stability is most certainly valuable in understanding the dynamical processes affecting a fluid, by itself such knowledge is often insufficient. While it is true that a statically stable fluid constrains vertical motions, other forces may be at work which oppose that constraint. For this reason two non-dimensional numbers were calculated at all experimental points at which static stability was measured. These were the Richardson number

$$Ri = \frac{g\bar{\alpha}\,\partial T/\partial z}{(\partial U/\partial z)^2}$$

and the Burger number

$$B = \frac{gd\bar{\alpha}\overline{\Delta_z T}}{(b-a)^2\Omega^2} = Ro_T \frac{\overline{\Delta_z T}}{\Delta T}.$$

Using the thermal-wind relationship we may express the Richardson number in the form

$$Ri = \frac{4\Omega^2}{g\bar{\alpha}} \frac{\overline{\Delta_z T}/\Delta z}{(\Delta_r T/\Delta r)^2} = \frac{4B}{(Ro_T)_i^2},$$

where $(Ro_T)_i$, the internal thermal Rossby number, is $gd\bar{\alpha}\Delta_r T/\Omega^2(b-a)^2$, $\Delta_r T$ is the radial temperature gradient across the interior of the fluid, and the other symbols are as defined in table 1.

For silicone oil and water, $\Delta_r T$ was assumed to be constant and equal to the maximum thermal wave amplitude, measured at the mid-depth and mid-radius along the traverse at $\Delta T = 5{\cdot}00\,^{\circ}\mathrm{C}$. This assumption was suggested by the observation that the static stability was essentially constant along that traverse, implying little change in the isothermal slope. For mercury, on the other hand, the static stability was observed to increase, implying that $\Delta_r T$ decreased, with decreasing rotation rate. Therefore $\Delta_r T$ was assumed to be equal to the thermal wave amplitude (in the regular wave regime) or the turbulent amplitude (in the non-geostrophic turbulent regime) at the individual data points at which computations were made.

As a result of these admittedly questionable, but necessary, assumptions, the quality of the Richardson number was poor. However, as it turned out, the differences in the values of Ri, as a function of the Prandtl number, were sufficiently large so that they were hardly affected by the particular choice of $\Delta_r T$.

Figure 19 shows Ri as a function of Ro_T for silicone oil, water and mercury. All data were measured at $\Delta T = 5{\cdot}00\,^{\circ}\mathrm{C}$. Data points corresponding to the upper symmetric regime in silicone oil and water are marked S, those corresponding to the non-geostrophic turbulent regime in mercury are marked T and those corresponding to the regular wave regimes are marked W, N, where N is the observed wavenumber.

For all three fluids, Ri decreases as Ω decreases (and Ro_T increases). For silicone oil, it ranges from approximately 300 in the fully developed wave regime ($Ro_T \doteq 0{\cdot}08$), to approximately 100 at the transition to the upper symmetric regime ($Ro_T \doteq 0{\cdot}2$), and continues to decrease, in a linear fashion, as Ro_T increases into the upper symmetric regime, to a value of approximately 30 at $Ro_T \doteq 0{\cdot}7$. For water, Ri ranges from approximately 100 in the fully developed wave regime ($Ro_T \doteq 0{\cdot}2$) to approximately 15 at the transition to the upper symmetric regime at $Ro_T \doteq 1$.† For mercury, Ri is approximately 5 deep within the regular wave regime at $Ro_T \doteq 0{\cdot}3$. As Ro_T increases, it slowly decreases to approximately 3 at $Ro_T \doteq 1$. The assumption of geostrophy (upon which the Richardson number computations are based) becomes progressively worse at higher values of Ro_T. We shall, nevertheless, quote two more computations: Ri decreases to

† These values of Ri, for water, agree very well with those reported by Fultz *et al.* (1959) for water with a free upper surface.

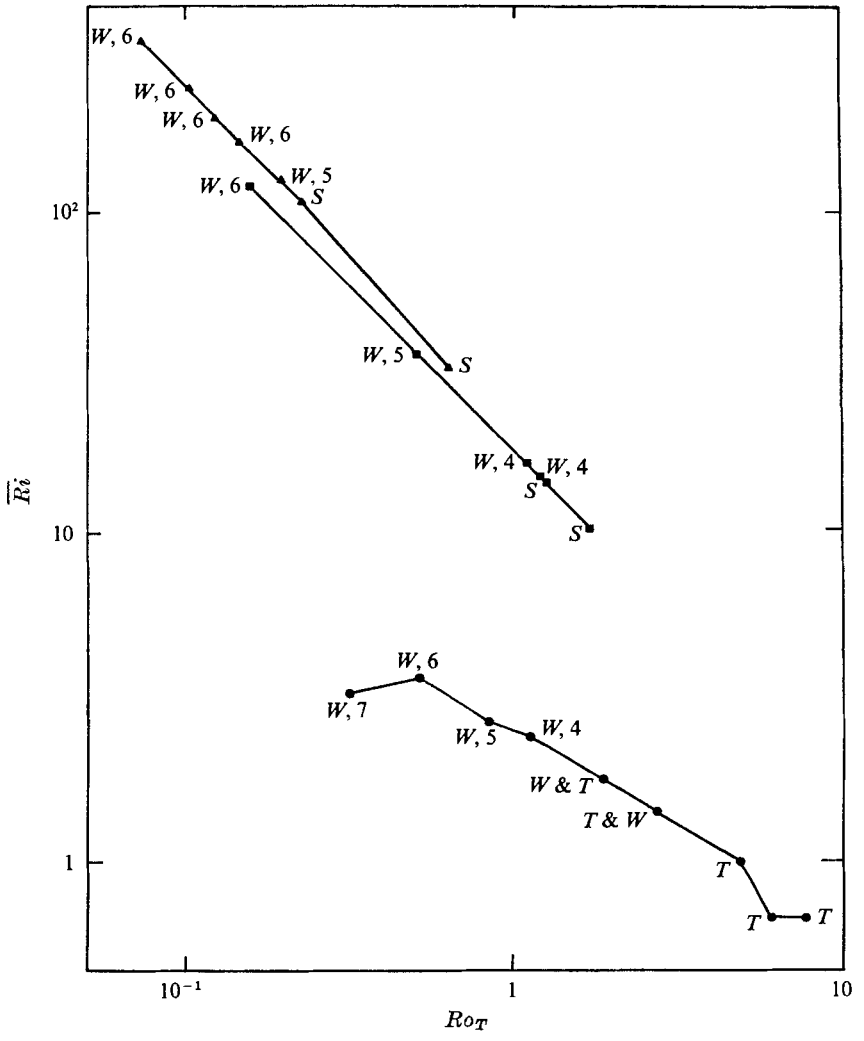

FIGURE 19. The Richardson number Ri as a function of the imposed thermal Rossby number Ro_T for silicone oil (triangles), water (squares) and mercury (circles) along a traverse across the regime diagrams at $\Delta T = 5{\cdot}00$ °C. The symbols next to each data point indicate the following: T, non-geostrophic turbulent convection; S, upper symmetric convection; W, N, baroclinic wave convection of wavenumber N.

approximately 2 in the vicinity of the zone of transition to turbulence ($Ro_T \doteq 3$), and further decreases, to approximately unity, within the non-geostrophic turbulent regime at $Ro_T \doteq 7$.

For silicone oil and water, Ri is linearly related to Ro_T. For mercury, the relation is less regular. However, no sharp changes are evident in the zone of transition to turbulence.

Figure 20 is a plot of the Burger number B as a function of Ro_T for silicone oil (triangles), water (squares) and mercury (circles). The symbols next to each data point describe the character of the convection at that data point, and were

	K	P	Nu	$\{PK\}$	τ
Onset value	86·9	251	2·08	4910	0·24
Final value	86·7	256	2·05	4780	0·27

TABLE 2. The values of K, P, Nu, $\{PK\}$ and τ at $Ra = 6500$ from runs F and $F1$. The upper row of values is taken at the time $t \simeq 2{\cdot}50$ from run F. The lower row is taken from the end of run $F1$.

the existence of time-periodic disturbances. This conclusion is consistent with the data for K and Nu in table 3 and the discussion in §6.2.

The values of τ in table 2 are virtually the same as those obtained previously for run C. The present values can be compared with previous experimental and theoretical results. From figure 9 of Willis & Deardorff (1970), the experimental value $\tau = 0{\cdot}32$ at $Ra = 6500$ is obtained. This value is best compared with the final value $\tau = 0{\cdot}27$, when the numerical disturbances were of finite amplitude. Theoretical values of τ can be found from figure 8 of Clever & Busse (1974). The value $\tau = 0{\cdot}23$ is obtained for $\lambda_y = \pi$, $\lambda_x = 2{\cdot}0$ and $Ra = 6500$. This value is best compared with the onset value, $\tau = 0{\cdot}24$, when the numerical disturbances were very small. Thus the numerical values of τ are in good agreement with experimental and theoretical results.

The energetics and dynamics of the disturbances are discussed in greater detail in appendix A, where the total flow field is separated into the mean flow (average taken along x) and the disturbance flow. Thus the total kinetic energy K is separated into a mean flow kinetic energy $\overline{K}$ associated with the rolls and a disturbance kinetic energy K' associated with the oscillations. The primary conclusions from appendix A are summarized in §7.

One result that can be discussed here is the relationship between τ and the mean flow kinetic energy $\overline{K}$. According to Busse & Whitehead (1974), the period τ is proportional to the circulation time of the mean flow. In the present problem the wavelength λ_y of the mean flow is held fixed. For this discussion, we assume that the spatial variation of the mean flow is virtually unchanged for modest changes in $\overline{K}$. Under these conditions, the statement by the above authors can be represented by the relation $\tau \propto \overline{K}^{-\frac{1}{2}}$. At the onset of the disturbances, $\tau = 0{\cdot}24$ and $K = \overline{K} = 86{\cdot}9$ as given in table 2. When the disturbances reach finite amplitude, $\tau = 0{\cdot}27$ and $\overline{K} = 62{\cdot}8$ (as given in figure 14). These two sets of values are compatible with the relationship $\tau \propto \overline{K}^{-\frac{1}{2}}$ to within 5 %.† Thus the present data also imply that τ is proportional to the circulation time of the mean flow.

5. Convection at higher Rayleigh numbers

The two remaining numerical solutions to be discussed are for the Rayleigh numbers $Ra = 9000$ and $Ra = 25\,000$. These calculations are denoted in table 1 as runs D and E. The initial conditions are as in run C, where $\mathbf{V} = 0$ and the temperature θ is given by (9).

† The same result is obtained if an extra decimal place is retained in the calculated values of τ.

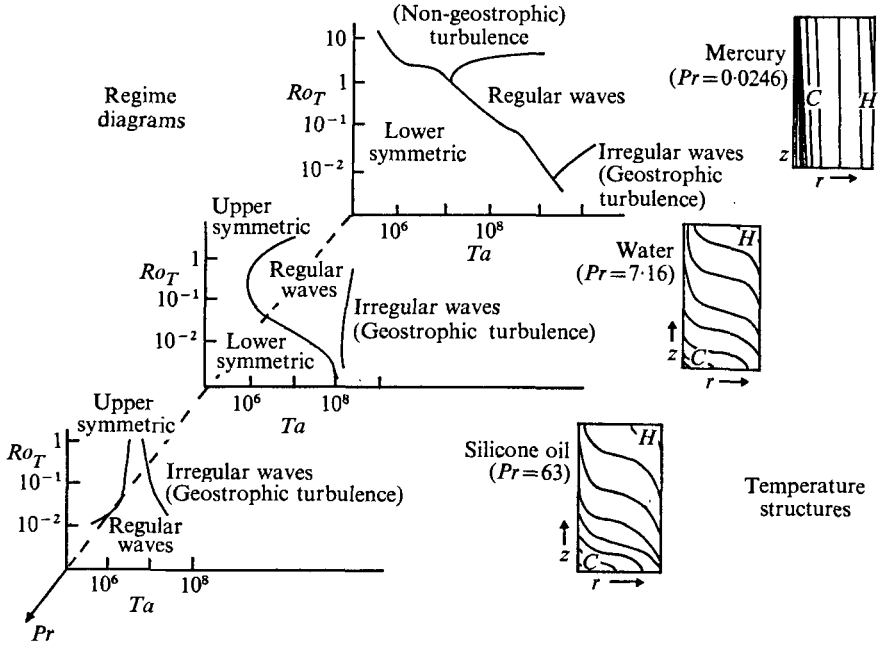

FIGURE 21. The regime diagrams for silicone oil, water (after Fein 1973) and mercury plotted in the three-dimensional space (Ro_T, Ta, Pr). To the right of the regime diagrams are shown meridional cross-sections of the zonally averaged temperature measured at ΔT = 5·00 °C approximately mid-way across the regular wave regime for each of the three fluids (see figure 17).

transition between waves and the *upper symmetric regime*, which is highly *convective* and has horizontally oriented isothermal surfaces. The regime diagram for water displays transitions between waves and both the upper and the lower symmetric regime.

As the Prandtl number increases there is a continual counter-clockwise turning of the boundaries separating the regular wave regime from the upper symmetric regime (the non-geostrophic turbulent regime in mercury) and the irregular wave regime. As a consequence, increasing the Rossby number results in a transition from *irregular* to *regular* waves in fluids with low Prandtl numbers and from *regular* to *irregular* waves in fluids with high Prandtl numbers. However, transitions to irregular waves, or geostrophically turbulent flows (such as are exhibited on atmospheric weather maps), occur within the range of Taylor numbers of interest only for fluids with Prandtl numbers sufficiently greater than unity.

This work is contribution no. 120 of the Geophysical Fluid Dynamics Institute, Florida State University. It was funded by the Office of Naval Research, under contract no. N00014-68-A-0159, and partially under the National Science Foundation grant no. DES 73-00558 A01.

REFERENCES

BARCILON, V. 1964 Role of Ekman layers in the stability of the symmetric regime obtained in a rotating annulus. *J. Atmos. Sci.* **21**, 291–299.

DOUGLAS, H. A. & MASON, P. J. 1973 Thermal convection in a large rotating fluid annulus: some effects of varying the aspect ratio. *J. Atmos. Sci.* **30**, 1124–1134.

FEIN, J. S. 1973 An experimental study of the effects of the upper boundary condition on the thermal convection in a rotating, differentially heated cylindrical annulus of fluid. *Geophys. Fluid Dyn.* **5**, 213–248.

FOWLIS, W. W. 1970 Techniques and apparatus for the fast and accurate measurement of fluid temperature and flow speed fields. *Rev. Sci. Instrum.* **41**, 570–576.

FOWLIS, W. W. & HIDE, R. 1965 Thermal convection in a rotating annulus of liquid: effect of viscosity on the transition between axisymmetric and non-axisymmetric flow regimes. *J. Atmos. Sci.* **22**, 541–558.

FOWLIS, W. W. & ROSSBY, H. T. 1964 A compilation of selected data on the temperature dependence of some physical properties of water, glycerol–water solutions and mercury. *Hydrodyn. Rotating Fluids Project, Dept. Geology Geophys. M.I.T., Lab. Note,* HRF/LN4.

FULTZ, D. 1956 A survey of certain thermally and mechanically driven fluid systems of meteorological interest. *Fluid Models in Geophysics*, pp. 27–63. U.S. Govt Printing Office.

FULTZ, D., LONG, R. R., OWENS, G. V., BOHAN, W., KAYLOR, R. & WEIL, J. 1959 Studies of thermal convection in a rotating cylinder with some implications for large-scale atmospheric motions. *Meteor. Monograph*, **4**. Boston: Am. Met. Soc.

HIDE, R. 1953 Some experiments on thermal convection in a rotating liquid. *Quart. J. Roy. Met. Soc.* **79**, 161.

HIDE, R. 1958 An experimental study of thermal convection in a rotating liquid. *Phil. Trans.* A **250**, 441–478.

HIDE, R. 1969 Some laboratory experiments on free thermal convection in a rotating fluid subject to a horizontal temperature gradient and their relation to the theory of the global atmospheric circulation. *The Global Circulation of the Atmosphere* (ed. G. A. Corby), pp. 196–221. London: Roy. Met. Soc.

HIDE, R. & MASON, P. J. 1975 Sloping convection in a rotating fluid. *Adv. in Phys.* **24**, 47–100.

MASON, P. J. 1976 Baroclinic waves in a container with sloping end walls. *Phil. Trans.* A (in press).